LBL-33028
UC-404

Lawrence Berkeley Laboratory
UNIVERSITY OF CALIFORNIA

Engineering Division

Growth and Characterization of Isotopically Enriched ^{70}Ge and ^{74}Ge Single Crystals

K. Itoh
(M.S. Thesis)

October 1992

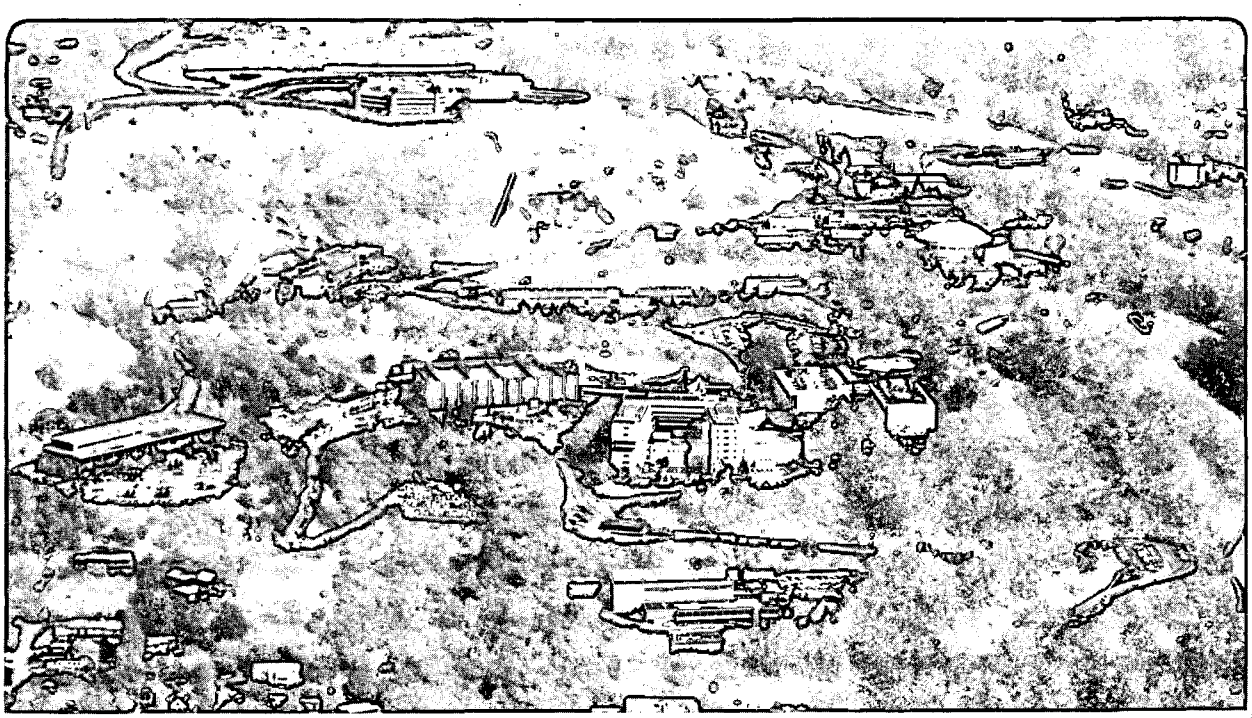

LOAN COPY
Circulates
for 4 weeks
Bldg. 50 Library.
Copy 2
LBL-33028

Prepared for the U.S. Department of Energy under Contract Number DE-AC03-76SF00098

DISCLAIMER

This document was prepared as an account of work sponsored by the United States Government. Neither the United States Government nor any agency thereof, nor The Regents of the University of California, nor any of their employees, makes any warranty, express or implied, or assumes any legal liability or responsibility for the accuracy, completeness, or usefulness of any information, apparatus, product, or process disclosed, or represents that its use would not infringe privately owned rights. Reference herein to any specific commercial product, process, or service by its trade name, trademark, manufacturer, or otherwise, does not necessarily constitute or imply its endorsement, recommendation, or favoring by the United States Government or any agency thereof, or The Regents of the University of California. The views and opinions of authors expressed herein do not necessarily state or reflect those of the United States Government or any agency thereof or The Regents of the University of California and shall not be used for advertising or product endorsement purposes.

Lawrence Berkeley Laboratory is an equal opportunity employer.

DISCLAIMER

This document was prepared as an account of work sponsored by the United States Government. While this document is believed to contain correct information, neither the United States Government nor any agency thereof, nor the Regents of the University of California, nor any of their employees, makes any warranty, express or implied, or assumes any legal responsibility for the accuracy, completeness, or usefulness of any information, apparatus, product, or process disclosed, or represents that its use would not infringe privately owned rights. Reference herein to any specific commercial product, process, or service by its trade name, trademark, manufacturer, or otherwise, does not necessarily constitute or imply its endorsement, recommendation, or favoring by the United States Government or any agency thereof, or the Regents of the University of California. The views and opinions of authors expressed herein do not necessarily state or reflect those of the United States Government or any agency thereof or the Regents of the University of California.

LBL-33028

GROWTH AND CHARACTERIZATION OF ISOTOPICALLY ENRICHED ^{70}Ge and ^{74}Ge SINGLE CRYSTALS

KOHEI ITOH

Engineering Science, Engineering Division
Lawrence Berkeley Laboratory, 1 Cyclotron Rd.
Berkeley, CA 94720
and
Center for Particle Astrophysics
Physics Dept., University of California
Berkeley, CA 94720

and

Materials Science and Mineral Engineering Department
University of California
Berkeley, CA 94720

October 1992

This work was supported by the US National Science Foundation Center for Particle Astrophysics through grant number ADT-8809616 and the U.S. Department of Energy under Contract No. DE-AC03-76SF00098.

Acknowledgement

I am especially grateful to my advisor, Professor Eugene E. Haller for setting up a wonderful learning opportunity through this research project. His continuous support has been a tremendous encouragement for my endeavors to pursue my graduate studies in the United State. I would like to extend many appreciations to the director of NSF Center for Particle Astrophysics, Professor Bernard Sadoulet, for his continuous interest in this project and for his careful review of this manuscript. Many invaluable comments by Professor Eicke Weber have also contributed to the completion of this thesis.

None of the present work would have been possible without the generous help of members of Prof. Haller's research group. The idea of the simple Ge crystal grower described in this thesis originates in Bill Hansen's 30 year long experience in this field. My efficiency in the lab was greatly improved by many practical suggestions by Jeff Beeman. Dr.Wladek Walukiewicz's deep knowledge of semiconductor physics has always been helpful. Dick Davis and Joe Guitron assisted me building apparatus and finding tools and parts lying somewhere in the lab. John Emes is the sample preparation specialist. Margaret Ragsdale has been extremely kind and efficient in performing the myriad of administrative tasks. Jeff Wolk was very patient in teaching me how to use the far infrared spectrometer. I acknowledge the kind support by members in the group: Dr. Franz Zach, James Heyman, Dave Bliss, In-Chi Wu, Amy Moll, Oscar Dubon and many others. I feel especially fortunate that I happened to start my graduate study at Berkeley with Amy and Oscar. They have been wonderful companions in overcoming the competitive coursework, preliminary exams and other difficulties in the lab.

Finally I'd like to extend my deepest appreciation to my family, especially my parants and my wife Yuko, for their warm support along the way.

I greatfully acknowlege the support of the the US NSF Center for Particle Astrophysics, through grant number ADT-8809616. I also thank the US Department of Energy for their support, through grant number DE-AC03-76SF00098.

Abstract

Isotopically enriched ^{70}Ge and ^{74}Ge single crystals were successfully grown by a newly developed vertical Bridgman method. The system allows us to reliably grow high purity Ge single crystals of approximately 1 cm^3 volume.

To our knowledge, we have grown the first ^{70}Ge single crystal. The electrically active chemical impurity concentration for both crystals was found to be $\sim 2\times10^{12}$ cm^{-3} which is two order of magnitude better that of ^{74}Ge crystals previously grown by two different groups. [1,2] Isotopic enrichment of the ^{70}Ge and the ^{74}Ge crystals is 96.3% and 96.8%, respectively. The residual chemical impurities present in both crystals were identified as phosphorus, copper, aluminum, and indium. A wide variety of experiments which take advantage of the isotopic purity of our crystals are discussed.

Table of Contents

1. Introduction 1

2. Purification and crystal growth of isotopically enriched Ge crystals 5

2.1. Purification 5

2.1.1. Zone refining method 5

2.1.2. Zone Refining of small quantity Ge (~100 g) 7

2.2. Crystal growth 10

2.2.1. Vertical Bridgman crystal growth 11

2.2.2. Small Ge (~4g) crystal growth system 12

2.2.3. Sample preparation procedure prior to the crystal growth 14

3. Characterization of isotopically enriched ^{70}Ge and ^{74}Ge single crystals 16

3.1. Isotopic composition measurement (SIMS technique) 16

3.2. Orientation of ^{70}Ge#4 and ^{74}Ge#2 crystals 17

3.3. Dislocation density 18

3.4. Net impurity concentration profiles of ^{70}Ge#4 and ^{74}Ge#2 crystals 21

3.5. Temperature dependence of free carrier concentration - variable temperature Hall effect measurement 22

3.6. Impurity identification - photothermal ionization spectroscopy 27

4. Summary 30

5. On Going and Future Experiments with Isotopically Controlled Ge 32

5.1. Neutron Transmutation Doping (NTD) Related Topics 32

5.1.1. Neutron Transmutation Doping (NTD) of Semiconductors 32

5.1.2. NTD Ge Thermistors 36

5.1.3. Compensation dependence of hopping conduction 39

5.1.4. Metal-Insulator (MI) transition. 40

5.1.4.1. Mott vs. Anderson transition in doped semiconductors 41

5.1.5. Electron Paramagnetic Spin Resonance (EPR) study of impurities in Ge 43
5.1.6. Study of the Se impurity in Ge 44
5.2. Phonon related topics 45
5.2.1. Isotope shift of the phonon frequency - Raman spectroscopy 45
5.2.2. Isotope shift of the band gap 47
5.2.3. Isotope shift of the heat capacity 50
5.2.4. Isotope shift of the thermal conductivity 50
5.2.5. Low temperature ballistic phonon transport - Phonon focusing 51
Appendix A: Effective distribution coefficient 52
Appendix B: Secondary Ion Mass Spectroscopy (SIMS) 54
Appendix C: Determination of crystal orientation by optical reflection 54
Appendix D: Dislocation etching 55
Appendix E: Net impurity profile measurement with the resistivity technique 55
Appendix F: Temperature dependence of the conduction mechanism in doped semiconductors 57
Appendix G: Photothermal ionization spectroscopy (PTIS) 63
Appendix H: EPR measurement 67
Appendix I: Determination of the isotope shift of the energy gap with the exiciton photoluminescence technique 69
References 70

1. Introduction

Along with the substantial progress of semiconductor science and technology, the control of the isotopic composition semiconductor materials has started to draw strong attention recently [1-7]. Because each element in the periodic table consists of a number of stable isotopes in fractions given by nature, the isotopic composition of all standard semiconductor materials is pre-determined unless a special isotope separation process is applied. However, it is well known that the isotopic composition of semiconductor materials can influence many basic physical parameters of the material [8.9]. Parameters which show such isotope effects include the lattice constant, the energy gap and all phonon related parameters (heat capacity, thermal conductivity, phonon propagation, etc.). Therefore, the investigation of the effect of various isotopes on fundamental solid state properties is of great scientific interest. To date the growth of only a few different types of isotopically enriched semiconductor crystals has been reported: ^{74}Ge single crystals [1,2] and ^{12}C and ^{13}C diamond single crystals [3-6]. With these crystals the isotope shift of the thermal conductivity [2,3], the energy gap [4,5], and the lattice constant [6,7] were measured.

In this masters thesis I will describe the purification, growth and characterization of chemically pure, isotopically enriched ^{70}Ge and ^{74}Ge single crystals. Our starting materials were isotopically separated ^{70}Ge and ^{74}Ge powders (~100g each) provided by Professor V. Ozhogin of the Kurchatov Institute in Moscow. The isotope separation was performed in Moscow by the gas centrifuge method similar to the one explained in Ref. 10. Because of the small starting quantities, a small volume zone refining technique and a special crystal growth system were developed. The very simple but effective ~4g Ge crystal growth systems will be discussed in detail in Sec. 2. The ^{70}Ge and ^{74}Ge crystals were characterized by 77K resistivity measurement, variable temperature Hall effect, photothermal ionization spectroscopy (PTIS) and chemical etching technique. The

characterization results will be shown in Sec. 3. Finally, Sec. 4 will summarize and conclude this masters project.

Because of its achievable high chemical purity and crystalline perfection, germanium continues to be one of the most suitable materials for nuclear radiation detectors [11], thermistors used for phonon-mediated detectors developed for dark matter searches and neutrino physics [12,13], cosmic ray background measurements [14], far infrared photoconductive detectors (Ge doped with Be, Ga, Zn, Cu, etc.) [15-17] and applications in other fundamental research in the field of solid state physics. The highest purity achieved in Ge is in the range of 10^9 electrically active impurities per cm^3 (compare with $4X10^{22}$ cm^{-3} Ge atoms!), while the purest Si and the GaAs is normally found to be on the order of $10^{11}cm^{-3}$ and $10^{12}cm^{-3}$ *, respectively.

Natural Ge consists of five stable isotopes with well known relative abundances: ^{70}Ge (20.5%), ^{72}Ge (27.4%), ^{73}Ge (7.8%), ^{74}Ge (36.5%) and ^{76}Ge (7.8%) [18]. Among these Ge isotopes, ^{70}Ge and ^{74}Ge were chosen for this project because they can be doped with shallow dopants by the neutron transmutation doping (NTD) technique. The ^{70}Ge crystal becomes Ga doped, i.e., p-type after the thermal neutron capture, while the ^{74}Ge turns n-type as a result of the As formation. The NTD technique is known as the best choice in achieving a homogeneous and random dopant distribution [19]. It should be noted at this point that Ge is the only common semiconductor material which produces both donor (n-type) and acceptor (p-type) through the NTD process. Other materials such as Si and GaAs can only produce n-type impurities through NTD. This may be a serious limitation for physical systems in which the ratio of n and p-type concentration, i.e., the compensation ratio is important.

In Sec. 5 I will describe various future experiments which will make use of these unique isotopically controlled Ge crystals. The first half of this section will start with the

* This result can only be achieved for liquid phase grown GaAs which leads to thin films only.

explanation of the NTD technique followed by a description of the NTD related projects. A few examples of the NTD related topics that will be covered in Sec. 5 are given below.

One primary goal of our project is to fabricate highly sensitive, isotopically controlled NTD Ge thermistors whose operation temperature lies in the range of 10 to 100 milliKelvin. The physics of semiconductor thermistors will be raised together with the discussion of the possible contribution of isotopically enriched Ge to the improvement of the thermistor resolution.

The homogeneity achieved with the NTD technique may also allow us to study semiconductor to metal transition phenomena over a wide range of compensation ratios. Because the same type of transition occurs in the multi-element, high T_c superconducting materials [20], the investigation of the metal-insulator transition phenomenon in simple semiconductors is expected to be important for an improved understanding of the superconducting mechanisms.

Isotopically controlled Ge will also allow us to explore many important impurity and defect properties that cannot be studied without this material. For example, the elimination of stable ^{73}Ge isotopes (nuclear spin I = 9/2) from Ge single crystals will improve the line widths in electron paramagnetic spin resonance (EPR) studies of defects in Ge. These studies may help the development of Ge based future devices (Si-Ge strained layers, etc.).

In the second half of Sec. 5 1 will discuss phonon related experiments such as the isotope related shift of the phonon frequency, the band gap, the heat capacity, etc. Various phonon related topics will be explained briefly with simple approximations of shifts we expect for each parameter.

Finally, it is worth mentioning that the ^{70}Ge and ^{74}Ge crystals grown in this work have already initiated several international, scientific collaborations. We have performed the Raman spectroscopy studies on the ^{70}Ge crystal [21] with Professor M. Cardona et al. at the Max-Planck-Institute in Stuttgart, Germany. The isotope shift of the band gap

between ^{70}Ge and ^{74}Ge is under investigation with Professor G. Davies et al. at King's College in London, England. (Preliminary results are presented in Sec.5.2.2). Other collaborations are under discussion.

2. Purification and crystal growth of isotopically enriched Ge crystals

2.1 Purification

We obtained 100g each of isotopically enriched ^{70}Ge and ^{74}Ge materials in a granular powder form. In order to determine the purity of these materials, one ^{70}Ge single crystal was grown without any purification. The impurity concentration in the crystal was so high ($>1X10^{17}cm^{-3}$, n-type) that it exhibited metallic conduction. Such donor concentrations are too high for most scientific experiments and purification is necessary.

2.1.1 The zone refining method

Zone refining [22] is the standard purification technique for many metals and semiconductors.* The method relies on the phenomenon of impurity segregation at the solid-liquid interface which is responsible for the impurity redistribution. Fig. 2.1 shows a schematic of the zone refining apparatus. A rod of Ge lies in a boat made of ultra-pure graphite. Either the sample area is evacuated or a continuous flow of a pure, non-reactive gas (N_2 or H_2) is supplied. An electro-magnetic field created by the RF heater couples to the graphite boat leading to a narrow, molten Ge zone. Moving the RF heater coil, the zone travels from one end to another at a slow, steady speed (~2mm/min in our case). As liquid Ge resolidifies, the motion of impurities across the solid-liquid interface is determined by

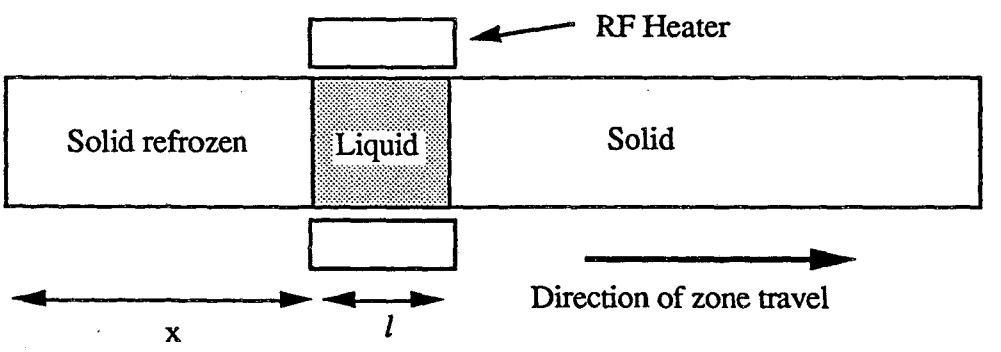

Fig. 2.1 Schematic of zone refining

1* The invention of the zone refining technique of 1953 was first applied to germanium [23].

the thermodynamically deduced distribution coefficient. The equilibrium distribution coefficient k_o for a particular impurity is defined as

$$k_o = C_S / C_L \tag{2.1}$$

where C_S is the impurity concentration in the resolidified Ge and C_L the concentration of the impurity in the Ge liquid. For the actual zone refining process, k_o should be replaced by the effective distribution coefficient k_{eff} since it is a non-equilibrium process. The definition and derivation of k_o and k_{eff} are given in Appendix A. When the effective distribution coefficient for a particular impurity is larger than 1, more solute atoms remain in the molten zone than in the solid. Thus with a movement of the molten zone, impurity atoms are transported to the end of the Ge rod where the final molten zone solidifies. When $k_{eff}>1$, the effect is opposite, and impurity atoms are transported to the starting end of the bar. Values of distribution coefficients for selected impurities in Ge are tabulated in Table 2.1. If the initial concentration C_o of the solute is uniform throughout the bar, the impurity concentration profile in the bar after one pass is:

$$\frac{C_S}{C_0} = \left[1 - (1 - k_{eff}) \exp\left(-\frac{k_{eff}}{l} x\right)\right] \tag{2.2}$$

where C_S is the concentration in the solid after a single pass, l the length of the molten

Table 2.1 Equilibrium distribution coefficient of various elements in Ge [24].

Element	k_{eff}
Boron	17
Aluminium	0.073
Gallium	0.087
Indium	0.001
Phosphorous	0.080
Aresenic	0.02
Antimony	0.0030
Copper	1.5×10^{-5}
Zinc	4.0×10^{-4}

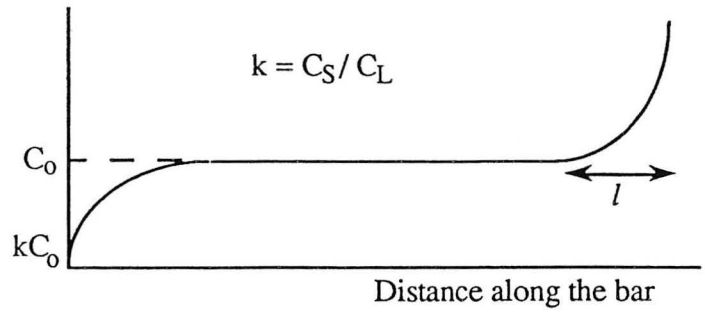

Fig. 2.2 Concentration profile afrter a single pass of zone refining

zone and x the length of the resolidified Ge solid. Fig. 2.2 shows the typical concentration profile for $k_{eff}<1$ after one pass. It is possible to repeat this process many times and achieve theoretically an infinitely small concentration of impurity atoms in the initial part of the Ge bar (if all impurities have $k_{eff}<1$). However, the interaction between the liquid Ge and the surrounding environment (boat, atmosphere) as well as impurity diffusion effects limit the ultimate impurity concentration to certain minimum levels. For example, even the purest graphite available may contain some impurities (P, B, Al, etc.), and the impurity transfer between the boat and the Ge seems to reach equilibrium when the concentration comes down to $\sim 10^{11} cm^{-3}$. The purest Ge bars ($10^9 \sim 10^{10} cm^{-3}$) are typically obtained by zone refining in a synthetic silica (SiO_2) boat.[25].

2.1.2 Zone Refining of a small quantity of Ge (~100 g)

Prior to the zone purification, it is necessary to transform the material into a continuous solid bar. It turned out that this process required some patience especially when the small quantity of 100g Ge needed to be shaped into a ~50cm long bar. During zone refining the partially melted Ge bar of a small cross section ($\sim 0.4 cm^2$) tended to separate into many drops because of the large surface tension of molten Ge. Nevertheless, this problem was solved by the careful adjustment of both the RF heater power and the tilt angle of the bar. The ultra-pure graphite boat shown in Fig. 2.3 was specially designed and

Fig. 2.3 Zone refining boat and a zone refined Ge bar

fabricated for this purpose. Along with the boat the zone refined Ge bar #746 (46cm long, 100g) is shown in Fig. 2.3. This bar originally contained ~$5\times10^{16}cm^{-3}$ gallium acceptor impurities. Fig. 2.4 shows Ga concentration profiles in Ge bar #746 measured after 1, 2, 3, 4 and 40 zone refining cycles. Assuming all carriers arise from Ga, the room temperature four point probe resistivity measurement was employed to determined the profiles after each of the first four passes. The bottom curve in Fig. 2.4 was measured at 77K in the dark by the resistivity technique. To reduce the total number of impurities, the impure end of the bar was removed twice between the 25th and the 40th passes. Therefore, the area under the curve (i.e., the total number of impurity) after 40 passes is significantly smaller than that of others. With Eq. 2.2 the distribution coefficient of the Ga for our refining system was calculated to be ~0.11. This is in good agreement with

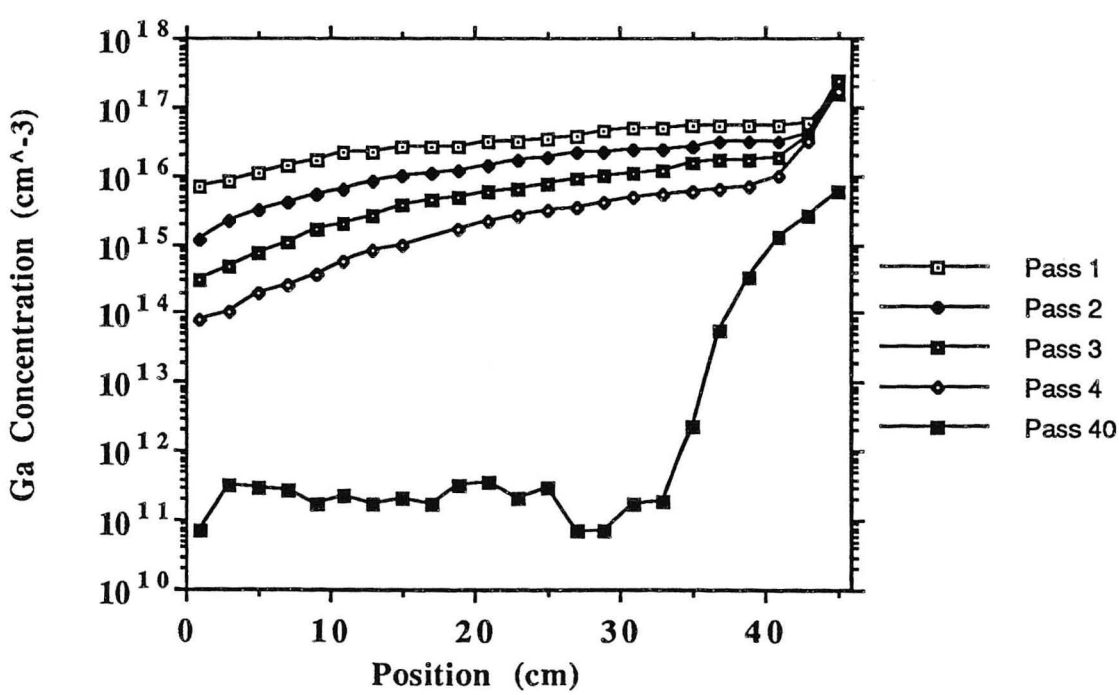

Fig. 2.4 Zone refining pass number evolution of the Ga concentration in the Ge bar #746

the equilibrium value of 0.087 listed in Table 2.1. Subsequently, the isotopically enriched materials were zone refined in the same fashion. Fig. 2.5 shows the result of the ~100g, ^{70}Ge bar impurity profile after 25 passes. Similar results were also obtained for the ^{74}Ge bar.

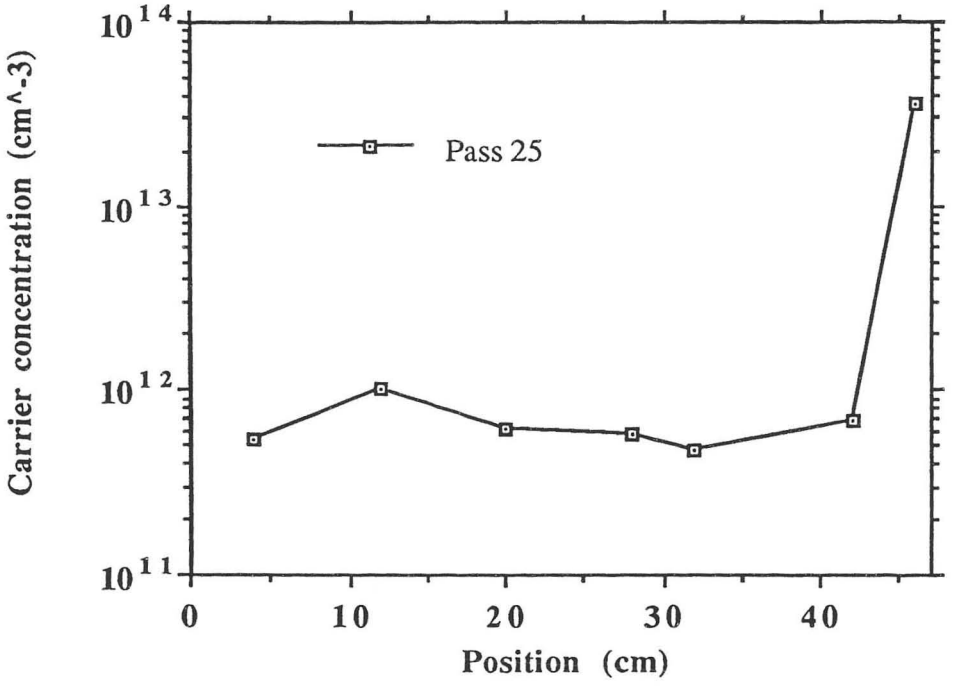

Fig. 2.5 Net carrier concentration profile of the 70-Ge bar after 25 zone refining passes

2.2 Crystal growth

In order to grow ~4 grams isotopically enriched Ge single crystals, the vertical Bridgman crystal growth method was chosen. Because it is very important to conserve the isotopic composition of the starting material, the use of a seed crystal made of natural Ge must have been avoided. This section describes the "seed-less" vertical Bridgman system which allows us to grow single crystals of pure Ge reliably.

2.2.1 Vertical Bridgman crystal growth

Fig.2.6 shows the schematic of the vertical Bridgman crystal growth process of Ge. After all the Ge in the crucible is melted, the temperature is slowly lowered from the bottom. With no seed crystals the initial nucleation with an arbitrary crystallographic orientation occurs at the bottom, narrow end of the crucible. A single crystal grows upward in the direction of the temperature gradient shown in Fig. 2.6. The growth interface is roughly situated at the melting temperature of Ge (T_m~936°C). This type of solidification is known as the normal freeze process. When a impurity with a distribution coefficient k is present in the starting material, the concentration profile of the impurity in the crystal grown by the equilibrium normal freeze process is given by

$$C_S(g) = k\, C_o\, (1 - g)^{k-1} \tag{2.3}$$

where C_S is the impurity concentration in the solid, C_o the original concentration in liquid, k the distribution coefficient, and g the fraction of melt which has been frozen. Since the actual crystal growth is a non-equilibrium process, Eq. 2.3 may only be used as an estimate.

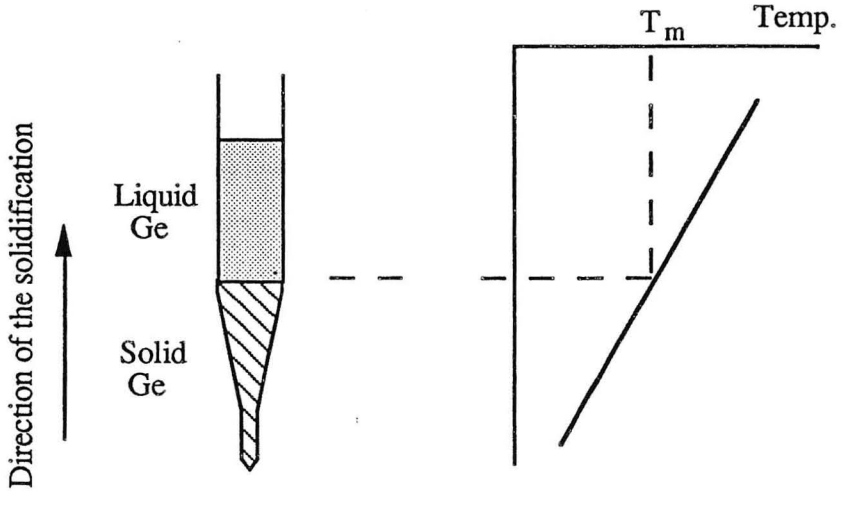

Fig. 2.6 Verticle Bridgman (Normal freezing) process

2.2.2 Small Ge (~4g) crystal growth system

The system developed in this work allows us to grow Ge single crystals of ~4 grams in weight. It is specifically designed for easy handling and rapid high purity growth. This system is designed such that it requires no seed crystal in order to preserve the isotopic purity of the starting material. The growth direction of the crystal cannot be chosen. The ability to control some important parameters for crystal growth (growth rate, interface temperature gradient, etc.) is limited because of the small dimension of the system. Nevertheless, after careful "trial and error" calibrations the system can reliably produce high purity single crystals. For high purity starting materials the net impurity concentration of $\sim 2 \times 10^{12} cm^{-3}$ is achieved in crystals grown with this system. This purity is very good especially for such a small crystal having a volume to surface ratio that is unfavorable for the exclusion of impurities. Besides the growth of high purity crystals, this method may be also used for the growth of crystals doped with various impurities. Whereas many expensive, large crystal growers must be dedicated to the growth of certain crystals in order to avoid cross-contaminations, this system can be inexpensively cleaned by simply changing one pair of quartz tubes and the graphite crucible.

Fig. 2.7 (a) shows the specially designed ultra-pure graphite crucible in the disassembled state. It consists of one pair of split molds and a cap. The crystal sits inside of the molds which are machined in the shape shown in Fig. 2.7 (a). In Fig.2.7 (b) we see the assembled crucible. In order to grow high purity crystals, the purity of the graphite plays a crucial factor. The graphite crucible used in this work was annealed at ~3000°C in a chlorine atmosphere to reduce the metal impurity contamination as far as possible [26]. Prior to the crystal growth, the interior of the split-off molds is coated with a thick carbon soot layer by using an oxygen-butane (C_4H_{10}) flame. The soft carbon layer acts as an cushion which provides the extra space of expansion when the molten Ge solidifies. Carbon is a neutral impurity in Ge and the solubility of C in Ge $\sim 10^{14}$ cm^{-3} near the melting

Fig. 2.7 Ultra-pure graphite crucible for a high purity Ge crystal growth.
(a) disassembled and (b) assembled

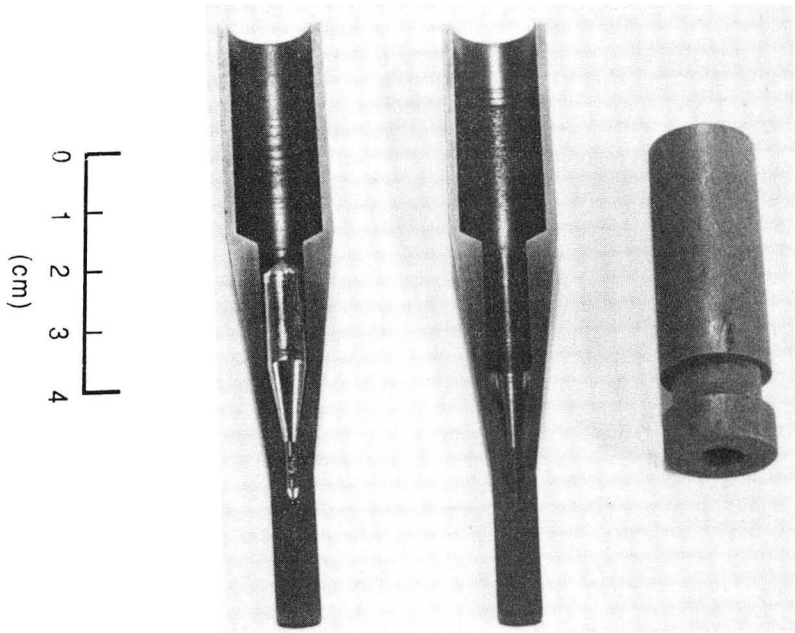

(a)

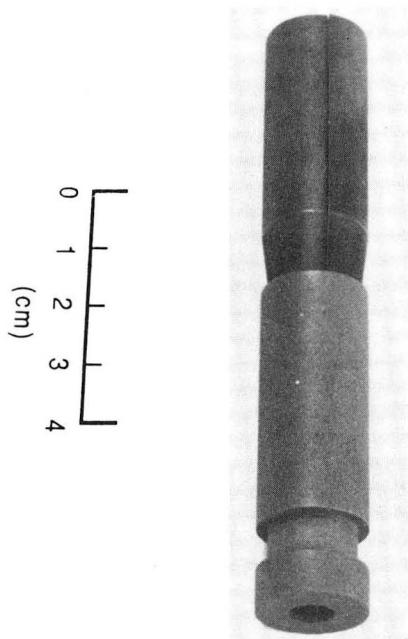

(b)

point [27]. Therefore carbon in direct contact with molten Ge is of no concern regarding purity. Fig. 2.8 shows the system developed for the crystal growth of isotopically enriched Ge crystals. The graphite crucible containing Ge starting material is placed inside the double-wall quartz tube. One end of the tube is closed, and crucible loading and gas feeding is performed through the open end. The diameter of the outer tube is roughly 3cm. The open end of the quartz tube is sealed by an "Ultra-torr" stainless steel fitting manufactured by Swagelock cooperation, USA. The crucible rests on the inner quartz support which is standing on the stainless steel fitting. The quartz tube is positioned inside the vertical furnace such that the crucible sits at a well calibrated position of the furnace. During heating forming gas is fed (mixture of N_2~1*l* /min and H_2~200cc/min) through the gas in valve in order to 1) avoid oxidation and 2) passivate impurities with hydrogen. The gas travels along the path shown by arrows in the figure and exits through the gas outlet valve. When the germanium inside the crucible is completely melted, the furnace temperature is slowly lowered. At the same time the flow rate of the gas is increased so that the gas hitting the bottom of the crucible creates a temperature gradient similar to that shown in Fig. 2.6. Consequently, a single crystal grows gradually from the bottom.

2.2.3 Sample preparation procedure prior to the crystal growth

Prior to the crystal growth of isotopically enriched ^{70}Ge and ^{74}Ge crystals, small pieces cleaved from the polycrystalline zone refined bar were treated in the following way;

(1) Etching in a HNO_3:HF (20:1) solution for 10 seconds to clean the surface.

(2) Washing with distilled and deionized (DDI) water

(3) Immersion in 10wt% KCN solution for a minute to remove any surface copper contaminations introduced by HNO_3 solution.

(5) Washing with DDI water

(6) Washing with distilled methanol.

(7) Blowing dry with a boil off nitrogen gun.

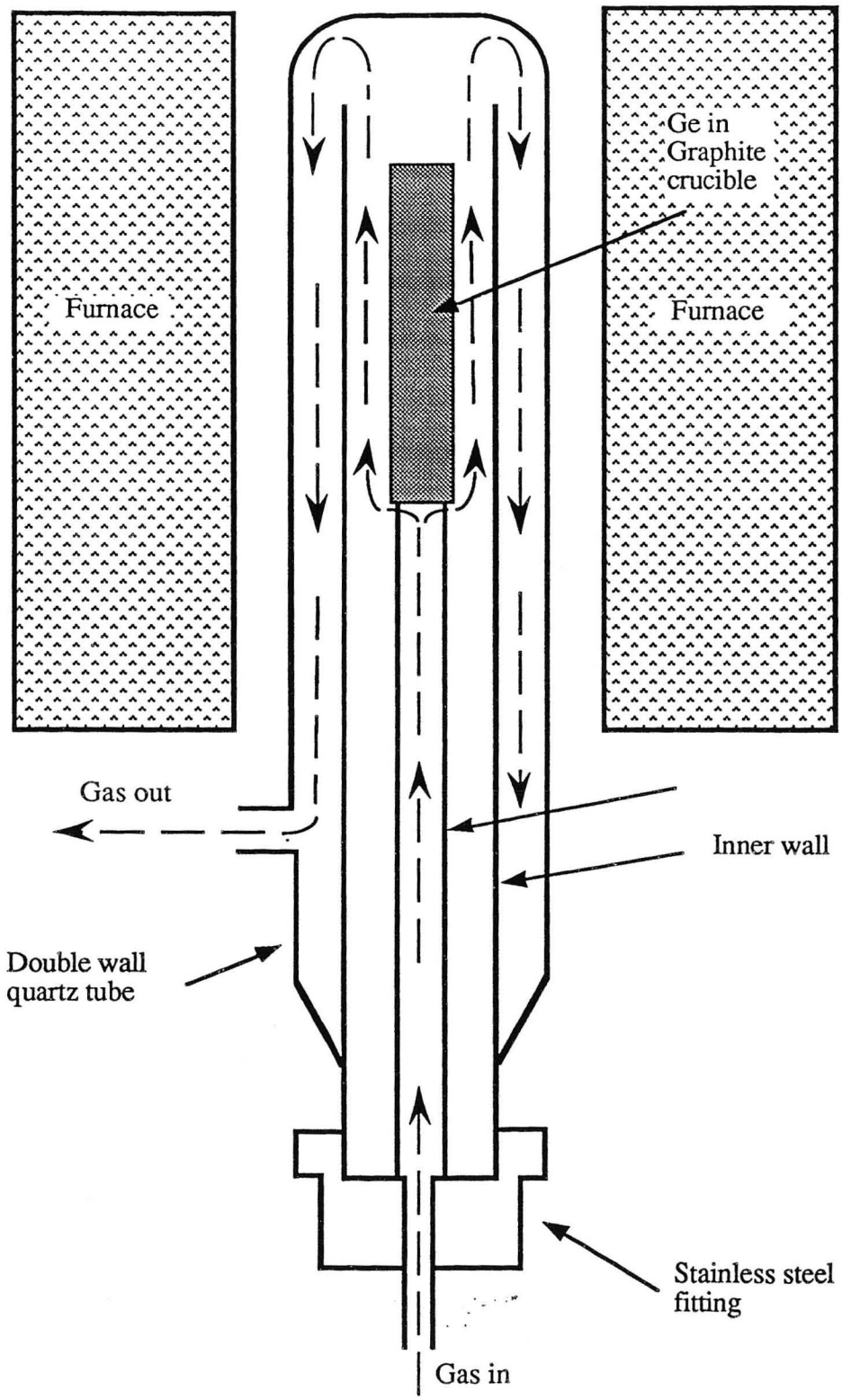

Fig. 2.8 Modified vertical Bridgman Ge crystal growth system

3. Characterization of isotopically enriched ^{70}Ge and ^{74}Ge single crystals

Fig. 3.1 is a photograph of isotopically enriched ^{70}Ge crystal #4 and ^{74}Ge crystal #2 grown by the method described in the previous chapter. A U. S. ten-cent coin is shown to give a scale. Both crystals are about 4 grams in weight, 6.5mm in diameter and 4.5cm in length. The following characterization measurements were performed on these crystals;

(1) Isotopic composition measurement (SIMS technique)

(2) Crystal orientation measurement (Optical reflection technique)

(3) Dislocation density (Chemical etching technique)

(4) Net impurity concentration profile along the growth direction
(Resistivity measurement)

(5) Temperature dependence of the free carrier concentration
(Variable temperature Hall effect)

(6) Impurity identification (PTIS technique)

3.1 Isotopic composition measurement (SIMS technique)

The isotopic composition of ^{70}Ge#4 and ^{74}Ge#2 crystals is found by secondary ion mass spectrometry (SIMS).*1 The result is shown in Table 3.1 together with the isotopic composition of natural Ge. Both ^{70}Ge#4 and ^{74}Ge#2 crystals were found to exceed an isotopic enrichment of 96%. With these enrichments it is possible to perform various new experiments which will be discussed in Sec. 5. Because no natural Ge was added during purification and growth, the isotopic composition of these crystals can be regarded as the isotopic composition of the starting granular powder Ge materials.

---

*1 See Appendix B for a brief explanation of this measurement.

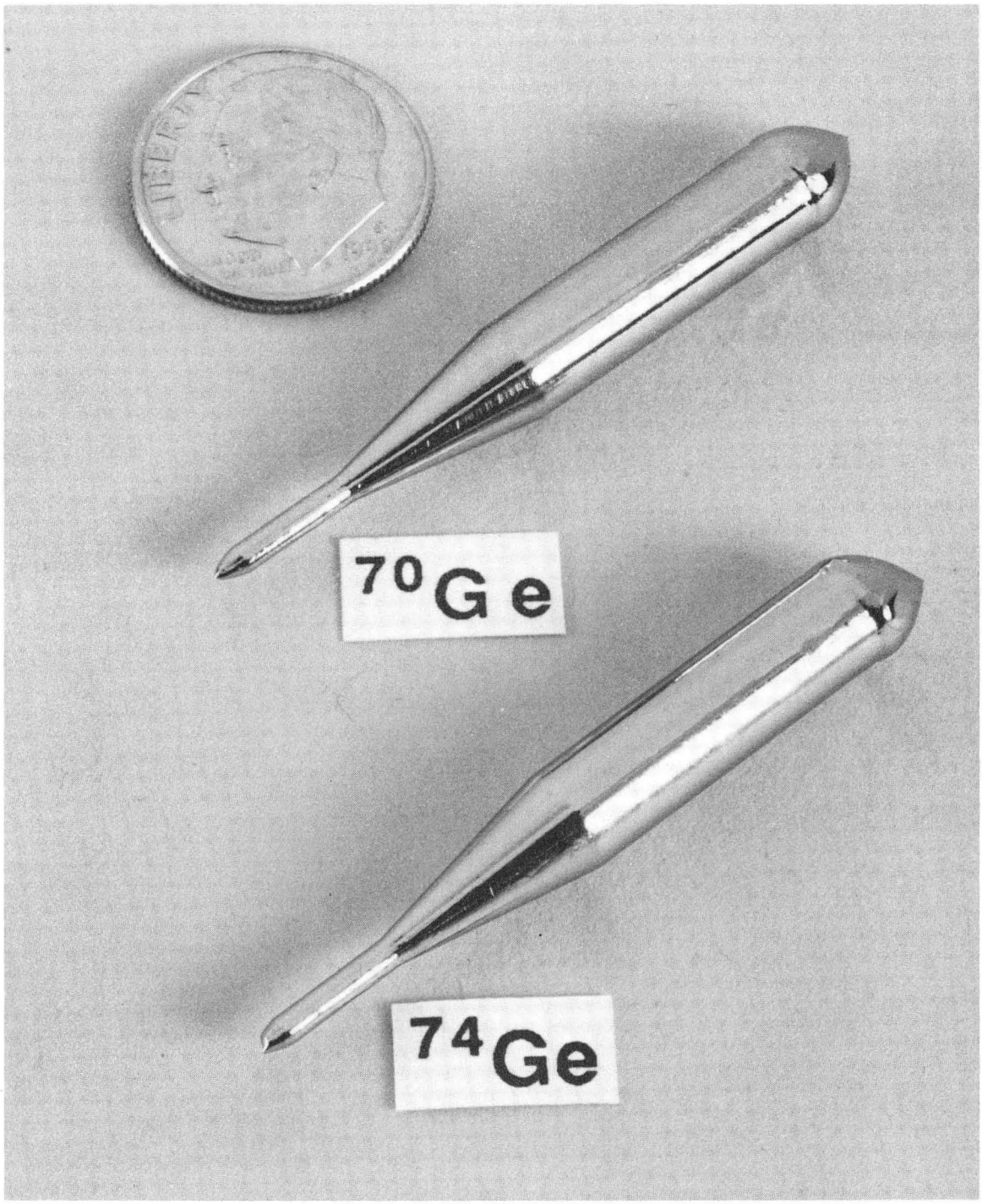

Fig. 3.1 Isotopically enriched ^{70}Ge crystal #4 and ^{74}Ge crystal #2

Table 3.1 Isotopic composition of ^{70}Ge#4 and ^{74}Ge#2 (unit: at.%)

Sample	^{70}Ge	^{72}Ge	^{73}Ge	^{74}Ge	^{76}Ge
Natural Ge	20.5%	27.4%	7.8%	36.5%	7.8%
^{70}Ge#4	96.3%	3.7%			
^{74}Ge#2	0.5%	0.17%	2.2%	96.8%	0.33%

3.2 Orientation of ^{70}Ge#4 and ^{74}Ge#2 crystals

Optical reflection measurements *2 revealed that the orientations of ^{70}Ge#4 and ^{74}Ge#2 crystal axes lie near <1 7 9> and <2 4 9>, respectively. The orientation measurements were necessary because both crystals were grown without seed crystals. Prior to the growth of the isotopically enriched crystals, more than seventy natural Ge crystals were grown by using the same method. After the statistical examination of the orientation distribution of these crystals, the <113> direction was found to be the preferred growth direction of crystals grown with this system. Indeed ^{74}Ge#2 came out near <113>. However there were many exceptions as one can see in the case of ^{70}Ge#4. Consequently the distribution of the single crystal growth orientations is quite broad.

3.3 Dislocation density

The dislocation densities in the ^{70}Ge#4 and ^{74}Ge#2 crystals were found by means of the chemical etching technique.*3 The ^{74}Ge#2 crystal was found to contain 10^3cm^{-2} dislocations distributed homogeneously. On the other hand, ^{70}Ge#4 possesses an inhomogeneous dislocation distribution, an average of 10^3cm^{-2} with two small highly dislocated spots (~10^5cm^{-2}) running along the crystal growth axis. Fig. 3.2 shows an example of the inhomogeneous dislocation distribution in the wafer cut from the natural Ge ingot #60 and grown by the same method. The average dislocation density of this wafer is

*2 Process of this technique is explained in Appendix C.
*3 See Appendix D for the procedure

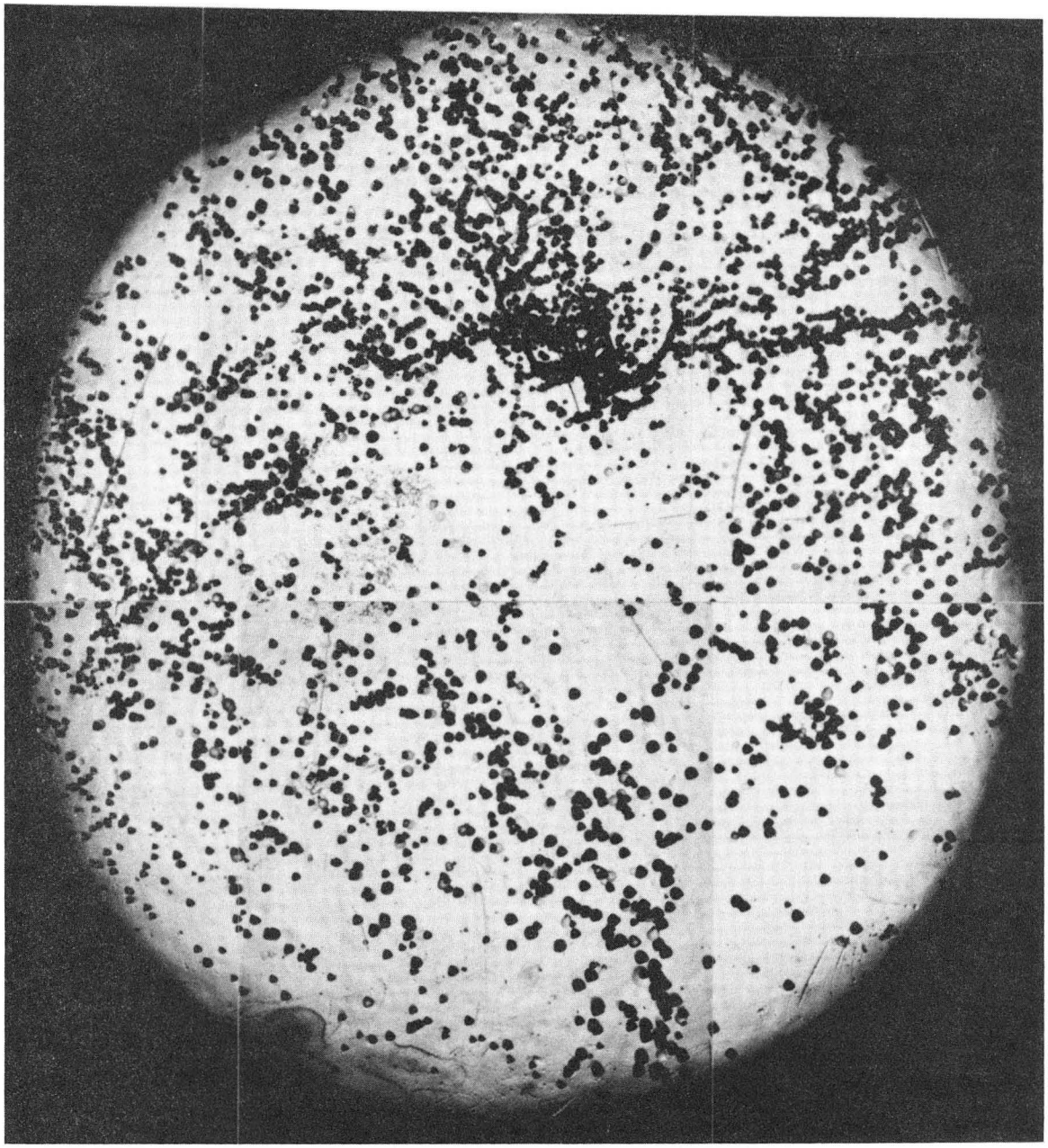

Fig. 3.2 Inhomogeneous dislocation distribution in the natural Ge crystal #60

estimated to be ~$10^3 cm^{-2}$ with one highly dense region corresponding to ~$10^5 cm^{-2}$. The study of dislocation distribution indicate the following potential sources for dislocations:

(1) External stress arising from the sticking of the solidifying Ge to the inner wall of the carbon crucible. (Therefore a careful carbon coating of the inner wall is necessary to avoid sticking.)

(2) Gas bubbles contained in the Ge liquid acting as stress sources during the solidification. (Evacuation of the growth system after melting is completed may be helpful in suppressing gas bubbles.)

(3) Carbon particles contained in the Ge liquid which are not able to escape to the surface during the Ge solidification.

The third source seems to be the least avoidable. Carbon was chosen to coat the inner wall of the crucible because its solubility in Ge solids is negligibly small. However, the growth rate of our system is rather rapid, and it may not allow all carbon particles to escape to the surface. Unfortunately the control of the growth rate is very difficult at present due to the small dimensions of the crystal. Therefore the complete elimination of the dislocation sources is yet to be achieved. Nevertheless, fifty percent of the last 40 crystals grown came out with a homogeneous 10^3 dislocations /cm^{-2} distribution.

Perfect dislocations in Ge have a Burgers vector a/2<110> and glide on {111} planes. Dislocation preferentially lies along <110>, and the Burgers vectors lie at 30° or 60° to the dislocation lines [28]. Once highly dislocated regions are created within the crystal, the propagation behavior of dislocations depends on the growth direction. As stated in the last section, <113> is the statistically most preferred growth direction. In this case dislocations lines are 30° off from the growth axis and they can grow out of the crystal. On the other hand, some crystals have their axes very close to the <110> orientation. Indeed this was the case for the ^{70}Ge#4 crystal in which two highly dislocated spots propagate along the growth axis all the way to the end. Therefore it is highly undesirable to grow crystals near <110> axis with this system.

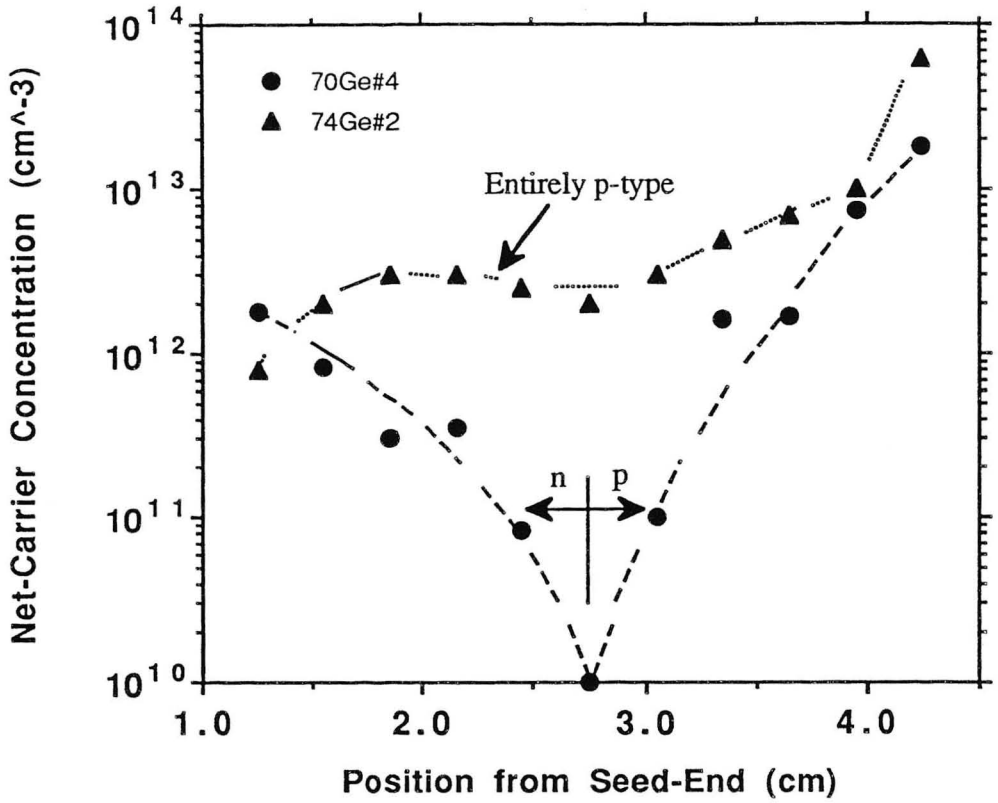

Fig. 3.3 Net impurity concentration profiles of crystals ^{70}Ge#4 and ^{74}Ge#2

3.4 Net impurity concentration profiles of crystals ^{70}Ge#4 and ^{74}Ge#2

To find the net-impurity concentration *4 profiles in crystals ^{70}Ge#4 and ^{74}Ge#2, resistivity measurements were performed.*5 The results displayed in Fig. 3.3 show that more than 70% of each crystal achieved a net-impurity concentration of the order of 10^{12}cm^{-3}. It was also found that ^{74}Ge#2 is entirely p-type whereas ^{70}Ge#4 contains a p-n-junction with p-type being on the growth end side. As stated in Sec. 2.2.1, the vertical Bridgman technique is a normal freeze process for which the concentration profile can be

*4 The net impurity concentration is defined by $|N_A-N_D|$ where N_A and N_D are acceptor and donor concentration, respectively.
*5 See Appendix E for the description of this technique

estimated by Eq. 2.3. Therefore, p-type impurities redistributed more to the growth end than n-type impurities in ^{70}Ge#4 implies that the effective distribution coefficient of p-type impurities is smaller than that of n-type impurities in this crystal. Referring to Table 2.1, we find indium to be the only shallow acceptor whose distribution coefficient is smaller than that of other shallow donors. However, it is also possible that deep acceptors (Zn, Cu, etc.) that have even smaller distribution coefficient than In were introduced during the growth process. In the following two sections it will be proved that the majority acceptor is indeed Cu. As shown in Table 2.1, Cu atoms, which have a very small k_0 value in Ge, were efficiently transported to the tail end of the crystals during the growth of ^{70}Ge#4 and ^{74}Ge#2.

3.5 Temperature dependence of free carrier concentration.

The temperature dependence of the free carrier concentration of four wafers cut from ^{70}Ge#4 and ^{74}Ge#2 was investigated by using the variable temperature Hall effect technique. The concept of variable temperature Hall effect technique will not be explained in this thesis since it is extensively covered in many textbooks [8,9,29,30]. By knowing the temperature dependence of the net-carrier concentration, one can obtain information such as the majority impurity concentration, the minority impurity concentration, the ionization energy of the majority impurity and the presence of deep levels. In order to obtain this information, it is necessary to understand the basic physics of temperature dependent electrical conduction in semiconductors.*5

Fig. 3.4 shows the temperature dependent free carrier concentration of two wafers cut from ^{74}Ge#2. Wafers ^{74}Ge#2-12 and ^{74}Ge#2-32 were cut at 1.8cm and 4.2cm from the seed end, respectively. They are both p-type, and the net impurity concentration results, 2×10^{12}cm^{-3} for ^{74}Ge#2-12 and 1×10^{14}cm^{-3} for ^{74}Ge#2-32, agree very well with

*6 The basic physics of the temperature dependence of the free carrier concentration and resistivity in semiconductors are given in Appendix F.

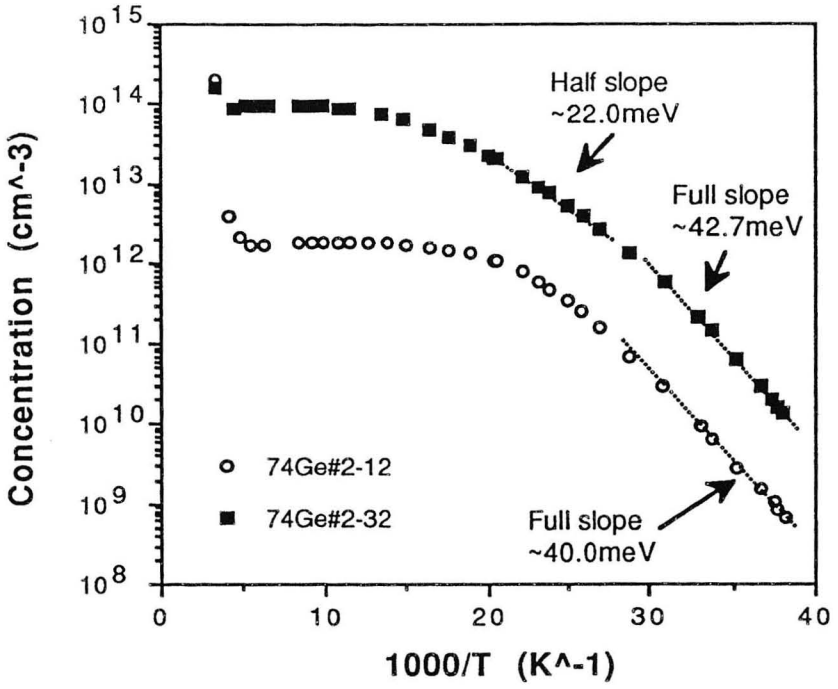

Fig. 3.4 Arrhenius plot of the free carrier concentration and the absolute temperature of the ^{74}Ge#2-12 and ^{74}Ge#2-32 samples

resistivity measurement shown in Fig. 3.3. The ionization energy of a majority impurity can be calculated from the slope of the freeze out curve as explained in Appendix F. Following this method, the ionization energies of the p-type impurity in both samples were calculated to be ~40meV. Comparing this result with the list of ionization energies for various accepters in Ge [24], we found copper (listed value 43meV) to be the most likely majority impurity. It is also seen in Fig. 3.4 that there are clear changes in slopes for both samples in the freeze out region in which the low temperature slopes are twice as steep as the higher temperature ones. Therefore the compensating donor concentration of ^{74}Ge#2-12 and ^{74}Ge#2-32 were found to be 2×10^{12}cm^{-3} and 3×10^{11}cm^{-3}, respectively. Fig. 3.5 shows the temperature dependence of the mobility of ^{74}Ge#2-12 and ^{74}Ge#2-32 samples

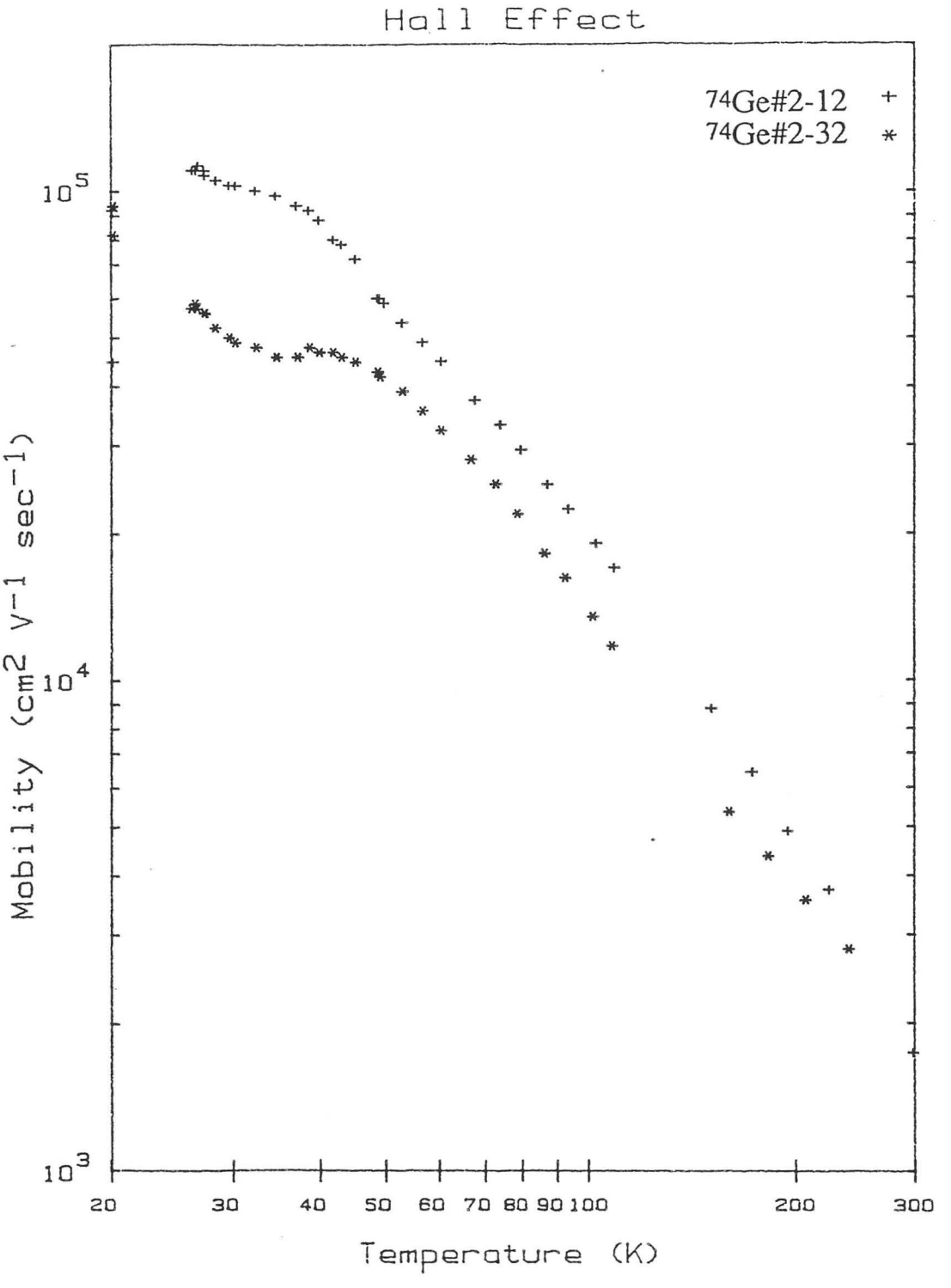

Fig. 3.5 Temperature dependence of the mobility in ^{74}Ge#2-12 and ^{74}Ge#2-32 samples

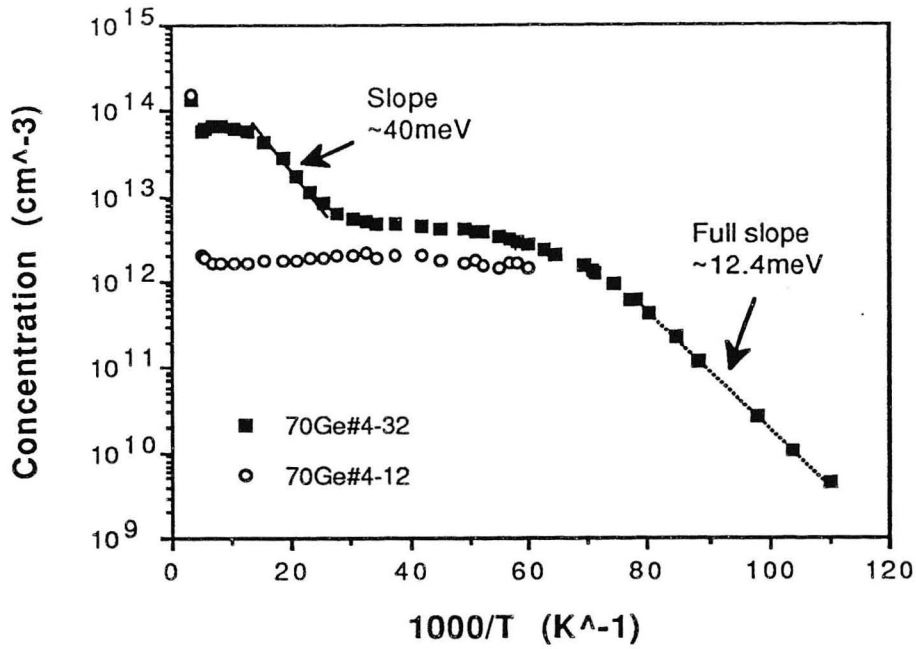

Fig. 3.6 Arrhenius plot of the free carrier concentration and the absolute temperature of the ^{70}Ge#4-12 and ^{70}Ge#4-32 samples

Fig. 3.6 shows the Hall effect result of two wafers cut from crystal ^{70}Ge#4. By the same token, ^{70}Ge#4-12 and ^{70}Ge#4-32 were situated at 1.8cm and 4.2cm from the seed end. This time ^{70}Ge#4-12 is n-type and ^{70}Ge#4-32 is p-type. Unfortunately n-type ohmic contacts prepared on ^{70}Ge#4-12 by the In(1%Sb) eutectic method failed to operate at temperatures below 20K. (Typically it is more difficult to fabricate n-type contacts on Ge than p-type boron implanted ohmic contacts for a low temperature operation.) Therefore it was not possible to find the compensation level and the ionization energy of the majority impurity in ^{70}Ge#4-12. However it can be still concluded that the net-impurity concentration of ^{70}Ge#4-12 is $2\times10^{12}cm^{-3}$, and the majority impurity is one of the shallow donors since the curve does not freeze out down to 20K. The ^{70}Ge#4-32 curve shows two big steps suggesting the presence of both shallow and deep acceptors. The concentration of deep acceptors is $7\times10^{13}cm^{-3}$ and of the shallow acceptors is $5\times10^{12}cm^{-3}$. Net-impurity

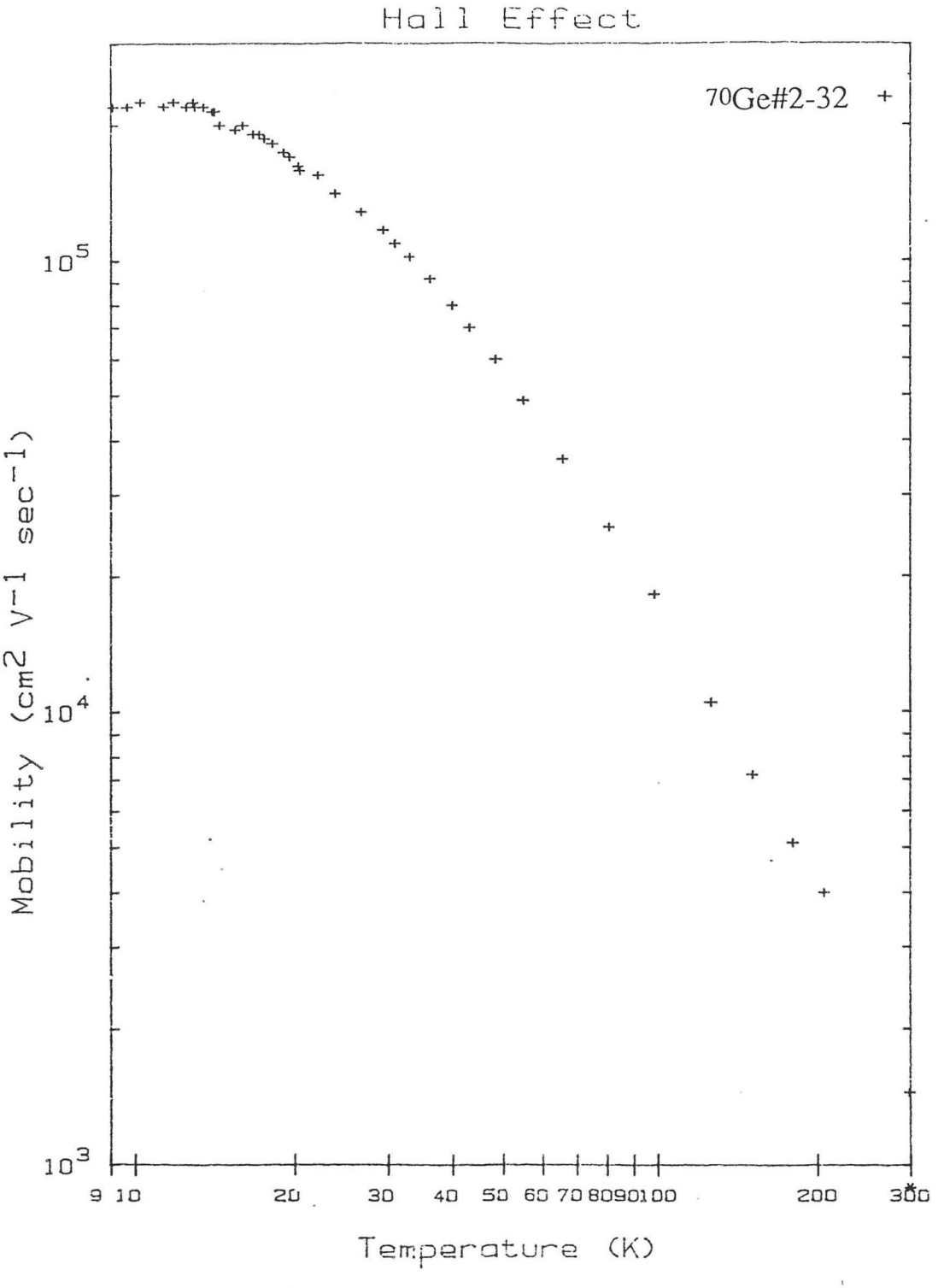

Fig. 3.7 Temperature dependence of the mobility in ^{70}Ge#4-32 sample

concentration results on ^{70}Ge#4-12 and ^{70}Ge#4-32 obtained by the Hall effect are also in a good agreement with the resistivity results in Fig. 3.3. The ionization energy of the shallow acceptor calculated from the slope is 12.4meV, which is a typical value for a hydrogenic impurity predicted by the effective mass theory. It is not possible to identify a half slope region in the freeze-out curve. This indicates that the compensating donor concentration is very close to the majority shallow impurity concentration of $5\times10^{12}cm^{-3}$. Fig. 3.7 also shows the temperature dependence of the mobility in ^{70}Ge#4-32 sample.

In a conclusion, the presence of the triple acceptor Cu was confirmed for both samples. Nevertheless 75% of both crystals achieved the net impurity concentration of low $10^{12}cm^{-3}$, which is comparable to the purest silicon available.

3.6 Impurity identification with PTIS

The photothermal ionization spectroscopy (PTIS) technique was employed to identify impurities in crystals ^{70}Ge#4 and ^{74}Ge#2. This technique is known to be extremely sensitive with detection limits of less than $10^{8}cm^{-3}$ shallow impurities in favorable cases. A short description of this technique is given in Appendix G. *6

Fig. 3.8 shows the PTIS spectrum obtained with ^{74}Ge#2-32. The positions of three peaks exactly match with the B, C, and D transitions of copper. This confirms unambiguously the presence of copper consistent with the result of the Hall effect measurements. No peaks due to Zn were observed in this PTIS measurement. Similar copper peaks were also observed in sample ^{70}Ge#4-32.

Fig. 3.9 shows the PTIS spectrum of ^{70}Ge#4-12. As seen in Fig.1.5, this sample is n-type with the net impurity concentration of $\sim2\times10^{12}cm^{-3}$. Although some peak positions are shifted possibly due to a stress within the crystal, the strong peak at 90 cm^{-1}

*6 For a detailed description of this method one should refer to Ref. 31-33.

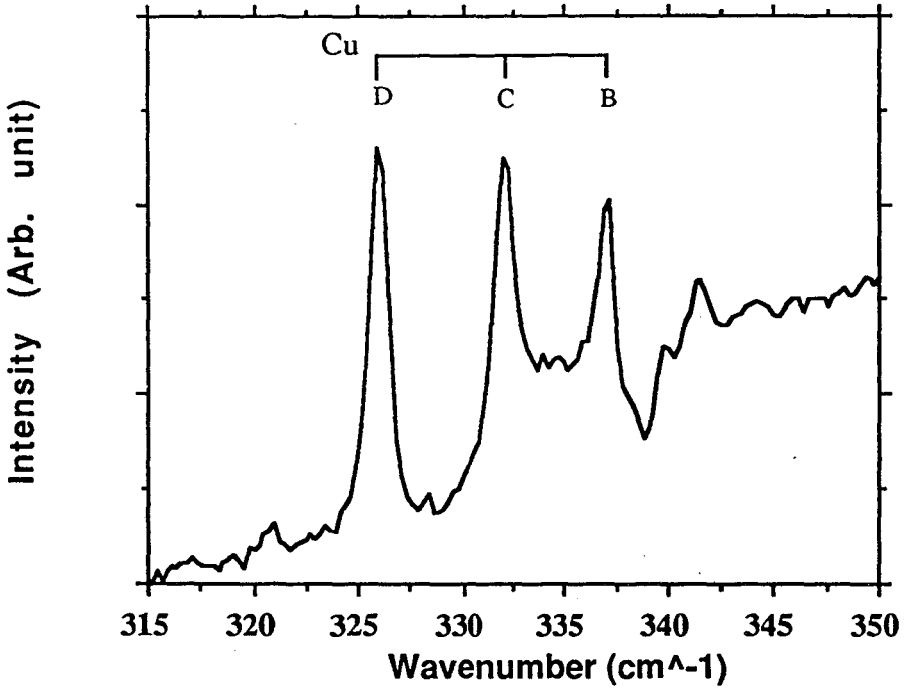

Fig. 3.8 PTI spectrum of ^{74}Ge#2-32

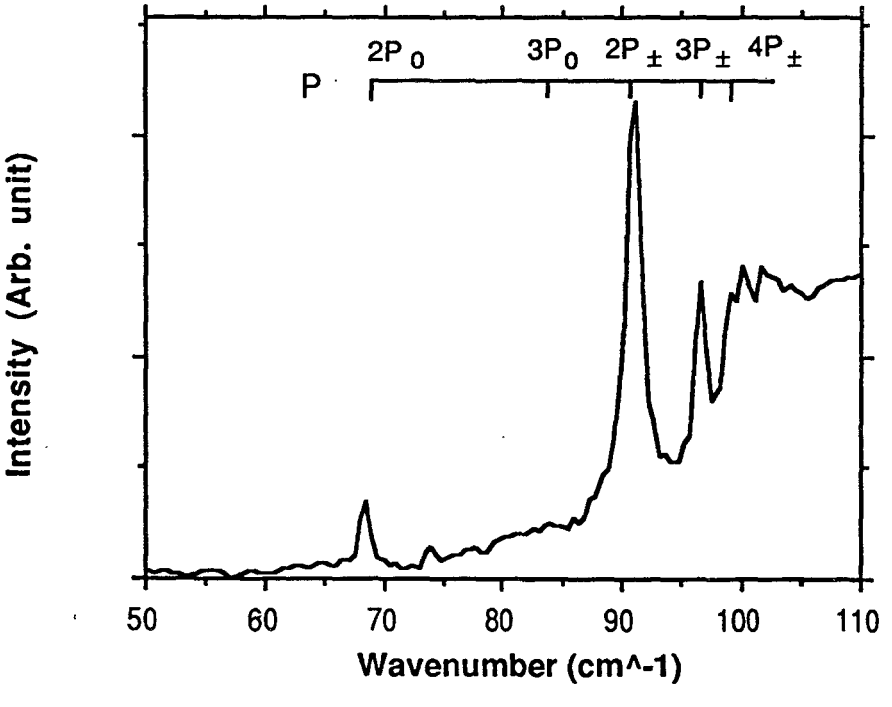

Fig. 3.9 PTI spectrum of ^{70}Ge#4-12

confirms the presence of phosphorus. Phosphorus was also found in ^{74}Ge#2 crystal.Because phosphorus was detected in most natural Ge crystals grown in the same system, its origin is thought to be in the growth system rather than in the starting material.

Lastly the shallow acceptors of ^{70}Ge#4-32 were examined. Fig. 3.10 shows the PTIS spectrum of the lower wave number range of ^{70}Ge#4-32. Many peaks are present, and each peak is assigned as shown in Fig. 3.10. The analysis shows that the shallow acceptors are aluminium with smaller amounts of gallium and indium.

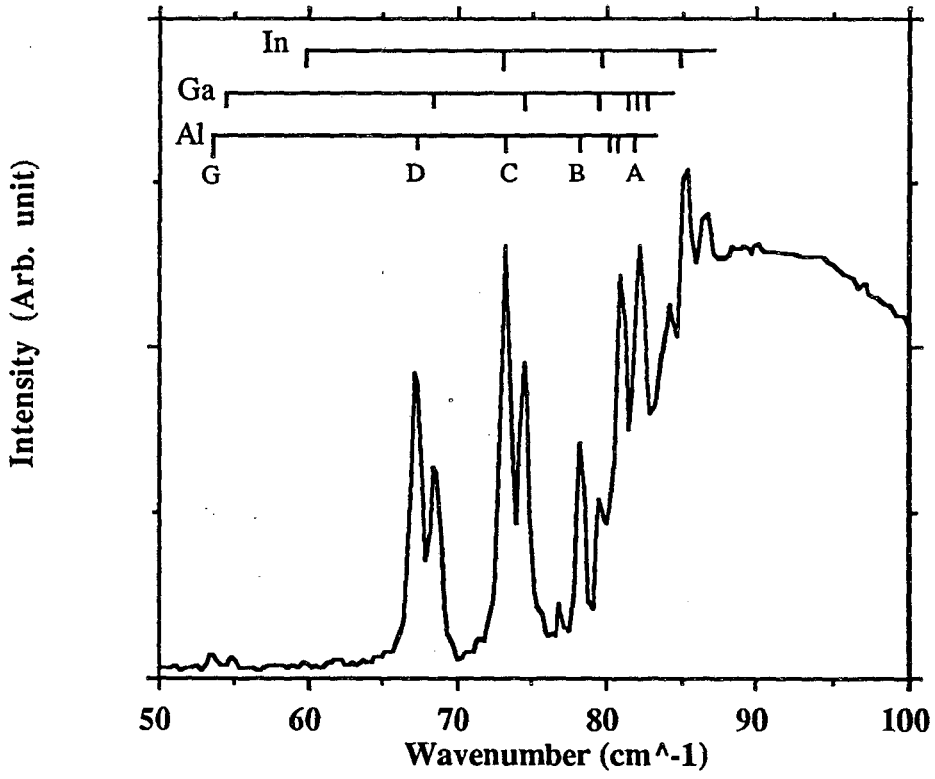

Fig.3.10 PTI spectrum of ^{70} Ge#4-32

4. Summary

Table 4.1 shows the summary of the characterization results on ^{70}Ge#4 and ^{74}Ge#2 crystals. The most important parameter, the "isotopic enrichment" was found to be over 96% in both crystals. The isotopic enrichment of the starting materials was conserved by the development of the growth system which did not require seed crystals.

In spite of the small size of the ingots (i.e., unfavorable surface to volume ratio for a high-purity crystal growth), nearly 75% of both crystals contain $2X10^{12}cm^{-3}$ residual net impurities which is two order of magnitude less than those of the ^{74}Ge enriched crystals previously grown by two different groups [1,2]. This was achieved by the zone purification and the careful cleaning and maintenance of the crystal growth system.

With these enrichments and purities, I believe that ^{70}Ge#4 and ^{74}Ge#2 crystals are suitable for a large number of the isotope effect related experiments in the fields of materials science and solid state physics. (Some will be explained in the following section.)

Although the vertical Bridgman crystal growth system we developed in this master's thesis project exhibited the ability to grow ^{74}Ge#2 which contained homogeneously distributed $\sim 10^3cm^{-2}$ dislocations, this result is not 100% reproducible. Once in a while crystals with inhomogeneous dislocation distribution are grown as already shown in Fig. 3.2. Elimination of dislocation sources and good control of the growth rate must be developed further in the future.

Both crystals were found to contain copper impurities. Although the Cu concentration is less than $2X10^{12}cm^{-3}$ in all the crystals grown by this system, Cu is a very fast diffuser and forms a triple acceptor in Ge. Therefore it is important to suppress Cu contamination as much as possible. Because natural Ge crystals purified by the same zone refining system but grown by different crystal grower do not suffer from Cu contamination, we know that the Cu source is located somewhere within the growth system developed for this project. The search for the Cu source must be continued.

Table 4.1 Summary of characterization results on ^{70}Ge#4 and ^{74}Ge#2

Crystal	^{70}Ge#4	^{74}Ge#2
Isotopic enrichment	96.3%	96.8%
Orientation	<179>	<249>
Dislocation density	10^3~10^5cm^{-2}	10^3cm^{-2}
Net impurity concentration (Pure side of the crystal)	2×10^{12}cm^{-3}	2×10^{12}cm^{-3}
Type (n or p)	n	p
Majority impurity	P	Cu
Minority Impurity	[Cu]<10^{12}cm^{-3}	[P]<10^{12}cm^{-3}
Other impurities (Total less than 10^{11}cm^{-3})	Al, Ga, In	Al, Ga, In

5. On Going and Future Experiments with Isotopically Controlled Ge

Isotopically controlled Ge crystals will provide an opportunity to investigate many interesting problems in materials science and solid state physics. This section is devoted to a description of experiments which will be possible because of the availability of this material. A brief background on experimental and theoretical aspects will also be presented. The following is a list of planned experiments:

1. Neutron Transmutation Doping (NTD) Related Topics
   - (a) NTD Ge thermistors - hopping conduction
   - (b) Metal-Insulator Transition
   - (c) Electron Paramagnetic Spin Resonance (EPR) study of impurities in Ge
   - (d) Study of selenium (Se) in Ge
   - (e) Selectively doped isotope superlattices
2. Phonon Related Topics
   - (e) Isotope shift of the phonon frequency - Raman spectroscopy
   - (f) Isotope shift of the band gap
   - (g) Isotope shift of the heat capacity
   - (h) Isotope shift of the thermal conductivity
   - (h) Low temperature ballistic phonon transport - Phonon focusing

5.1 Neutron Transmutation Doping (NTD) Related Topics

5.1.1. Neutron Transmutation Doping (NTD) of Semiconductors

The neutron transmutation doping (NTD) technique is a well established method for obtaining uniform and homogeneous dopant distributions in semiconductor materials [15]. During NTD the semiconductor materials are irradiated with thermal neutrons. While a

large number of thermal neutrons travel unhindered through the crystal, a few are captured by the host semiconductor material. When a neutron is captured, the new neutron to proton ratio in the nucleus may not be stable. An unstable nucleus decays by β^+ and β^- emission or electron capture. The new elements created by this process act as impurities or dopants in the substrate. Their identity depends on the original host isotope and the decay mode. The reactions of stable isotopes after capture of thermal neutrons for natural Si, Ge and GaAs crystals are shown in Table 5.1. For example, natural Si consists of three stable isotopes ^{28}Si, ^{29}Si and ^{30}Si present in a given concentration ratio. Applications of the NTD process to Si yields the reactions displayed in Table 5.1, i.e., ^{28}Si, ^{29}Si, ^{30}Si nuclei become ^{29}Si, ^{30}Si, ^{31}P, respectively. The important reaction is $^{30}Si \rightarrow {}^{31}P$ since phosphorus acts as a donor in Si. Obviously, the two other reactions $^{28}Si \rightarrow {}^{29}Si$ and $^{29}Si \rightarrow {}^{30}Si$ do not change the electronic property of the original Si material because ^{29}Si and ^{30}Si are stable isotopes. Thus, the NTD technique results in Si doped with P atoms.

In general, the impurity concentration (N_X) due to a particular isotope following NTD is given by:

$$N_x = \rho \, x_{Iso} \, \sigma_c \, n \tag{5.1}$$

where ρ is the number density of host semiconductor atoms (cm^{-3}), x_{Iso} is the abundance of the particular isotope, σ_c is the thermal neutron capture cross section of each nucleus (cm^2), and n is the fluence of thermal neutrons (cm^{-2}). The most significant feature of the NTD method the "uniformity" is due to the completely random distribution of the various host isotopes in the semiconductor crystals and the very small capture cross section of each nucleus as tabulated in Table 5.1 (1 barn = 10^{-24} cm^2). Because the capture cross section of each isotope is very small, most of the thermal neutrons travel through the sample without interacting with nuclei. Therefore the probability of a nuclear reaction is nearly equal everywhere in the crystal. A good example of application of NTD are a high-voltage, high-power silicon controlled rectifiers for which uniform doping is crucial [19].

Table 5.1 NTD Process in Silicon, Germanium and Gallium Arsenide

Silicon (Si)

Isotopes	Abundance (%)	σ_c (barn)	Neutron Capture and Reactions	Dopant Type
${}^{28}_{14}Si$	92.3		${}^{28}_{14}Si(n,\gamma)\ {}^{29}_{14}Si$	
${}^{29}_{14}Si$	4.7		${}^{29}_{14}Si(n,\gamma)\ {}^{30}_{14}Si$	
${}^{30}_{14}Si$	3.1	0.108	${}^{30}_{14}Si(n,\gamma)\ {}^{31}_{14}Si \rightarrow \beta^-, T1/2=2.62\ hr \rightarrow\ {}^{31}_{15}P$	n

Germanium (Ge)

Isotopes	Abundance (%)	σ_c (barn)	Neutron Capture and Reactions	Dopant Type
${}^{70}_{32}Ge$	20.5	3.25	${}^{70}_{32}Ge(n,\gamma)\ {}^{71}_{32}Ge \rightarrow EC, T1/2=11.2days \rightarrow\ {}^{71}_{31}Ga$	p
${}^{72}_{32}Ge$	27.4	1.0	${}^{72}_{32}Ge(n,\gamma)\ {}^{73}_{32}Ge$	
${}^{73}_{32}Ge$	7.8	15.0	${}^{73}_{32}Ge(n,\gamma)\ {}^{74}_{32}Ge$	
${}^{74}_{32}Ge$	36.5	0.52	${}^{74}_{32}Ge(n,\gamma)\ {}^{75}_{32}Ge \rightarrow \beta^-, T1/2=82.2min \rightarrow\ {}^{75}_{33}As$	n
${}^{76}_{32}Ge$	7.8	0.16	${}^{76}_{32}Ge(n,\gamma)\ {}^{77}_{32}Ge \rightarrow \beta^-, T1/2=11.3hr \rightarrow\ {}^{77}_{33}As$	
			${}^{77}_{33}As \rightarrow \beta^-, T1/2=38.8hr \rightarrow\ {}^{77}_{34}Se$	n

Gallium Arsenide (GaAs)

Isotopes	Abundance (%)	σ_c (barn)	Neutron Capture and Reactions	Dopant Type
${}^{69}_{31}Ga$	60.1	1.7	${}^{69}_{31}Ga(n,\gamma)\ {}^{70}_{31}Ga \rightarrow \beta^-, T1/2=21.1min \rightarrow\ {}^{70}_{32}Ge$	n
${}^{71}_{31}Ga$	39.9	4.6	${}^{71}_{31}Ga(n,\gamma)\ {}^{72}_{32}Ga \rightarrow \beta^-, T1/2=14.1hr \rightarrow\ {}^{72}_{32}Ge$	n
${}^{75}_{33}As$	100	4.4	${}^{75}_{33}As(n,\gamma)\ {}^{76}_{33}As \rightarrow \beta^-, T1/2=26.3hr \rightarrow\ {}^{76}_{34}Se$	n

Unfortunately, the type of dopants resulting from the NTD process cannot be determined arbitrarily since it solely depends on the available stable isotopes in the host semiconductor. For example, Si and GaAs can only be doped with n-type impurities. On the other hand Ge is unique because it contains isotopes which decay into both acceptors and donors. The isotope composition of natural Ge is such that the compensation ratio, K, in NTD natural Ge is fixed at:

$$K = \frac{N_{As} + 2N_{Se}}{N_{Ga}} \approx 0.32 \tag{5.2}$$

where N_{As}, N_{Se}, N_{Ga} are the concentration of As, Se, and Ga, respectively. However, the compensation ratio of NTD Ge can be controlled by changing the isotope composition of the starting Ge material. Therefore, it would be advantageous to grow isotopically controlled Ge and therefore determine the compensation ratio. Ge also has a further advantage over Si and GaAs in terms of the achievable purity as already stated in Sec. 1. The most interesting isotopes of Ge from the NTD point of view are ^{70}Ge and ^{74}Ge, since they decay to the well understood shallow impurities Ga and As, respectively. By combining ^{70}Ge and ^{74}Ge in various concentration ratios (from pure ^{70}Ge to pure ^{74}Ge), a series of samples with well defined compensation can be generated.

Lastly, in the interest of completeness, three shortcomings of the NTD process shall be stated;

(1) Fast neutrons leads to radiation damage. (Complete elimination of the fast neutrons in the reactor is impossible or impractical for the necessary neutron fluencies)

(2) Long duration of exposure to the thermal neutrons may induce secondary reactions such as $^{70}Ge \rightarrow {}^{71}Ga \rightarrow {}^{72}Ge$ and $^{74}Ge \rightarrow {}^{75}As \rightarrow {}^{76}Se$.

(3) Fast neutrons may also lead to radioactive spallation products (e.g., ^{68}Ge from n, 3n reaction of ^{70}Ge) which maybe detrimental in some astrophysical detector applications.

Thermal annealing at the appropriate temperature is usually sufficient to repair the lattice damage created by fast neutrons [34-36]. The secondary reactions produced from ^{70}Ge and ^{74}Ge nuclei are ^{72}Ge and ^{76}Se. Obviously, ^{72}Ge does not cause any problem but ^{76}Se is a double donor in Ge. Nevertheless, the amount of ^{76}Se produced is usually negligible at the standard doping levels.

5.1.2 NTD Ge Thermistors

The term "thermistor" refers to a device which reproducibly changes its resistance with a change of temperature. Thus, after proper calibration, one can measure the temperature increase caused by photons absorbed by the thermistor. In general, temperature is directly related to the energy of the incident photons ($E \sim k_B T$, k_B: Boltzman constant). In this sense, one can regard a thermistor as an energy sensor. A typical electrical circuit for semiconductor thermistors is shown in Fig. 5.1. The system is maintained at an appropriate temperature and the temperature increase of the thermistor due to the energy of incident particles is detected by the change in the resistance. A constant sensing current I is applied so that the change in resistance can be determined by the change in the voltage drop ΔV_S across the thermistor. Fig. 5.2 shows the temperature dependence of resistivity of NTD Ge in the milliKelvin range [37]. The higher resistivity samples with steep slopes are lightly doped whereas the low resistivity samples are heavily doped. In all cases, the starting material was natural Ge resulting in a fixed compensation ratio (p-type, $K \sim 0.32$). The low temperature conduction mechanism which is responsible for the temperature dependence of all the of NTD Ge samples shown in Fig. 5.2 is "variable range

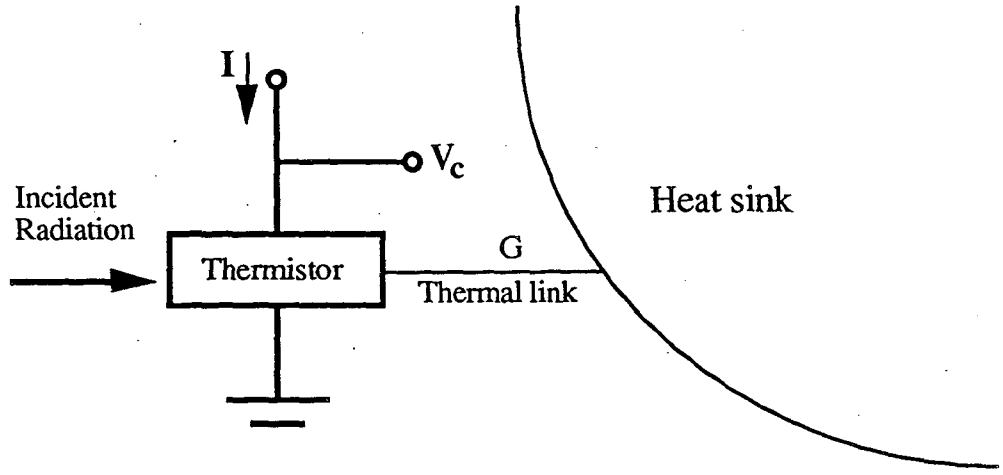

Fig. 5.1 Electrical circuit for a thermistor. In order to maintain its operating temperature, the thermistor is thermally connected to the heat sink through a thermal link of conductance G

hopping conduction".*1 Variable range hopping conduction theory predicts the following temperature dependence of the resistivity ρ for doped germanium; [38,39]

$$\rho = \rho_0 \exp\left(\frac{T_0}{T}\right)^{\frac{1}{2}} \tag{5.3}$$

where ρ_0 and T_0 are parameters which depend on dopant concentration and compensation ratio. Eq. 5.3 can be rewritten as,

$$\ln \rho = T_0^{1/2}\ T^{-1/2} + \ln \rho_0 \tag{5.3'}$$

Therefore, the slope of each curve in Fig. 5.2 is $T_0^{1/2}$ while the ln ρ axis (y-axis) intersection value is given by ρ_0. The sensitivity of the thermistor depends on the slope ($T_0^{1/2}$). Because one measures resistivity to obtain the temperature, the steeper the slope (larger value of T_0), the higher the sensitivity. It is also important to "design" the resistivity curve so that the resistance stays within the optimum range (10^5~$10^7\Omega$) for an electronic measurement given by the amplifier in the temperature range of interest. In order to obtain the desired ln ρ - $T^{1/2}$ dependence, ρ_0 and T_0 must lie within a certain range of

*1 See appendix F for a description of the hopping conduction in semiconductors.

values. For example, thermistors which operate in ~30mK range require a slope as steep as possible while maintaining the resistivity between 10^3 and 10^6 Ωcm. Thus, the control of both dopant concentration and the compensation ratio are crucial since ρ_0 and T_0 strongly depend on them. As stated earlier the compensation of the natural NTD Ge is fixed at 0.32. Therefore, isotopically controlled NTD Ge whose acceptor and donor concentration can be controlled independently may lead to materials with significantly improved thermistor sensitivity.

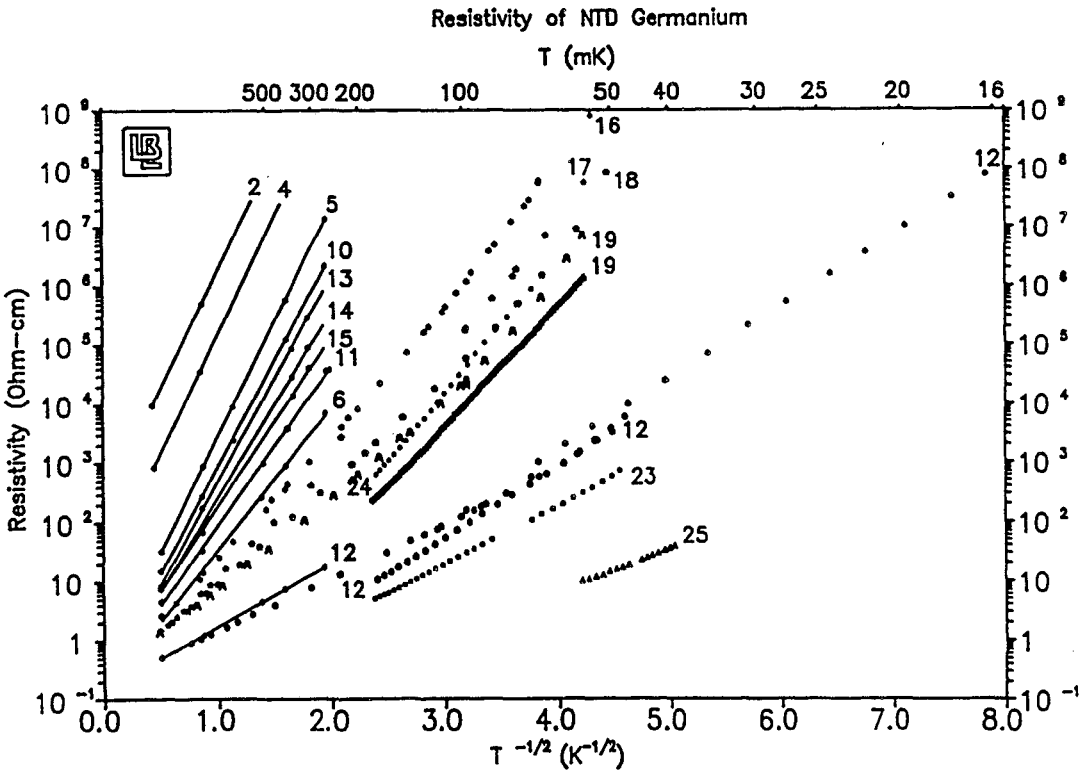

Fig. 5.2 Temperature dependence of resistivity of NTD Ge in the milliKelvin range

5.1.3. Compensation dependence of hopping conduction

The values of the two constants ρ_0 and T_0 in Eq. 5.3 depend on the dopant concentration and the compensation ratio. The concentration dependence of hopping conduction has been extensively studied since the early 1960s [40]. However, only a few groups have considered the compensation dependence of hopping conduction [41-43]. Davis and Compton studied the compensation dependence of the nearest neighbor hopping conduction with Ge:Sb in 1965 [43].*2 They found the resistivity ρ to be a minimum when $K \sim 0.4$ and ρ to increase approximately parabolically for $K \rightarrow 0$ and $K \rightarrow 1$. This result is easily understood because with $K \sim 0$, nearly all donor sites are filled with electrons and there are not enough empty donor sites for electrons to hop into. Similarly, when $K \sim 1$, nearly all donor sites are empty and the number of conducting electrons goes to zero. Davis and Compton also deduced the compensation dependence of ρ_0 and the activation energy for a hopping (E_A) in Eq. F.2 in Appendix F. Their result has served as an excellent qualitative guidance for other researchers who worked in this field. However, it is important for fabrication of thermistors to obtain quantitatively reliable data of the both nearest neighbor and variable range hopping conductions. The data obtained by Davis and Compton may be improved by the following measurements:

1) The lowest temperature they used was 2 K, i.e., at this temperature only the nearest neighbor hopping conduction still dominates. In order to obtain data for variable range hopping conduction, it is necessary to go to lower temperature.
2) The compensating centers in their case were deep acceptor defects which resulted from fast neutron irradiation. Thus the precise structure of the defects was unknown. There could have been deep donor formations affecting their results. Therefore, a sample which contains well defined dopants such as shallow

*2 See Appendix F for a description of the nearest neighbor hopping conduction.

hydrogenic majority and minority impurities is desirable for obtaining quantitative data.

3) The Ge:Sb they investigated was prepared by growth from a doped melt. The uniformity of the dopant distribution of melt doped crystals is known to be much worse than that of the NTD method. An inhomogeneous Sb distribution (striation) may have been present due to fluctuations in the segregation coefficient caused by local fluctuations in melt flow near the growth interface. The remelting temperature fluctuations lead to growth velocity changes which in turn affect the effective segregation coefficient.

The first conductivity measurement of isotopically enriched Ge was performed by Shlimak et al. with a NTD ^{74}Ge:As (~98% enriched) crystal [1]. The compensation ratio K of their crystal was 0.0027. However, the measured values of ρ_0 as a function of the arsenic concentration fluctuate strongly and we assume there must have been some unaccounted problems in their measurements. Theoretically, NTD isotopically controlled Ge should provide the ideal sample in terms of doping control, i.e., it is a ideal sample for a quantitative study of the compensation dependence of hopping conduction.

5.1.4 Metal-Insulator (MI) transition.

Increase of the dopant concentration in semiconductors eventually leads to an overlap of impurity electron wave functions. The overlap allows electrons to move rather freely from one impurity site to another without special excitation, resulting in a resistivity which is independent of the temperature. This is called "metallic conduction" in semiconductors. The subject of the interest is how the transition from semiconductor to metallic occurs. Is the conductivity continuous or abrupt across the transition ? At what impurity concentration should the transition occur ? These common questions in the field of "metal-insulator (MI) transition" have been intensively studied with various semiconductor systems [38]. Two of the major difficulties in the study of the MI transition

in semiconductors have been the production of samples with a microscopically homogeneous impurity distribution and the precise control of compensation. It has been also difficult to determine the compensation accurately when K is greater than 0.2. However, NTD Ge crystals consisting of ^{70}Ge and ^{74}Ge isotopes in a well controlled ratio will have excellent homogeneity in the dopant distribution and well defined compensation assuming an accurate knowledge of the neutron capture cross sections of each isotope.

5.1.4.1 Mott vs. Anderson MI transition in doped semiconductors

In 1949, Mott described the metal-insulator transition by imagining a crystalline array of hydrogen-like atoms with a lattice constant that could be varied [44]. He predicted that a discontinuous, abrupt MI transition with varying concentration should occur when

$$n^{1/3} a_H = 0.2 \tag{5.4}$$

where n is the number of electrons per unit volume and a_H the hydrogen radius. In the case of a semiconductor which is doped with hydrogen-like shallow impurities, one can apply the same type of equation

$$n^{1/3} a^* = 0.27 \tag{5.5}$$

where a^* is the Bohr radius of the shallow impurity center which is given by

$$a^* = \frac{h^2 \kappa}{4 \pi^2 m^* q^2} \tag{5.6}$$

where $\kappa=4\pi\varepsilon_r \varepsilon_o$. In Eq. 5.6, h is Planck's constant, m^* the effective mass, q the charge, ε_r the relative dielectric constant of the medium, and ε_o the permitivity of free space. The value 0.27 in Eq. 5.5 was determined experimentally and it applies to a wide variety of uncompensated materials as summarized by Edwards and Sienko [45].

However, in 1958, Anderson pointed out that the effect of random positioning of impurities must be taken into account when considering the MI transition of a disordered system [46]. In the framework of the "scaling theory" developed by Anderson et al. [47],

the critical behavior of zero temperature conductivity $\sigma(0)$ as the transition is approached from the metallic side is described by the form;

$$\sigma(0) = \sigma_0 \left(\frac{n}{n_c - 1}\right)^{\alpha} \quad . \quad \text{where } \alpha = 1 \tag{5.7}$$

where σ_0 is the prefactor, n the concentration, n_c the transition concentration, and α=1 the critical exponent. Thus, the Anderson MI transition is a continuous transition as seen in Eq. 5.7.

Therefore, there are two different types of MI transition: Mott type (first order transition) and Anderson type (second order transition). All the doped semiconductor systems so far investigated, compensated or uncompensated, have shown continuous MI transition and support the Anderson model. Particularly, compensated semiconductors showed clear Anderson transitions because of the disordered potential due to the ionized compensating centers.

In Eq. 5.7, the power factor α was predicted to be 1 by Anderson et al., and this was observed with various compensated semiconductors such as Ge:Sb [48], Si:P, B [49], etc.). However, the MI transition in uncompensated materials differed slightly from the complete theory of Anderson's: although transitions were always continuous, unpredicted value of α~1/2 in Eq. 5.7 were observed in nearly uncompensated Si:P [50], Si:As [51,52], Si:As, P [53], Si:B [54,55] and Ge:Sb [48].

Because Mott's abrupt transition may be seen as the α=0 case in Eq. 5.7, the reduction of α in the uncompensated materials may be due to the increase of the Mott-like MI transition component in the Anderson type MI transition.

However, no sample is entirely uncompensated. There are always some residual impurities in the semiconductor crystals which compensate the dopants. Thermodynamically favorable clustering of majority impurities near the MI transition may also lead to "self-compensation" [56]. Nevertheless, it will be extremely interesting to investigate the MI transition with isotopically pure NTD ^{70}Ge and ^{74}Ge crystals, because

the minority carrier concentration will be five orders of magnitude less than the majority carrier MI transition concentration and the microscopic distribution of the dopants will be completely uniform. It may be possible to investigate the ratio of the Mott-like and the Anderson-like components in the nearly ideal uncompensated semiconductor. It will also be interesting to investigate the effect of various compensation ratios on the MI transition phenomena by mixing ^{70}Ge and ^{74}Ge in a controlled fashion.

5.1.5 Electron Paramagnetic Spin Resonance (EPR) study of impurities in Ge

Among the various semiconductor defect characterization techniques, Electron Paramagnetic Spin Resonance (EPR) spectroscopy has been a very powerful when applicable [57,58]. The EPR technique provides microscopic information about impurities and defects such as their symmetry, the value of the nuclear spin of the impurity atom, the nuclear spins of neighboring host lattice atoms, the radius of the localized wave functions, the effect of external stress, etc. In general, most semiconductor crystals are macroscopically diamagnetic. However, if impurities or defects in semiconductors contain an unpaired electron the crystals become paramagnetic. The paramagnetic unpaired electrons associated with impurities or defects are the subjects of the EPR study. A brief discussion of EPR is given in Appendix H.

Table 5.1 shows the abundance of the stable isotopes in natural Si, Ge, and GaAs. Among them, isotopes with nuclear spins are ^{29}Si (I=1/2), ^{73}Ge (I=9/2), ^{69}Ga (I=3/2), ^{71}Ga (I=3/2) and ^{75}As (I=3/2). The rest do not have nuclear spin. Because of the superhyperfine interaction, it is desirable for atoms of the host crystal not to have a nuclear spin as explained Appendix G, . This problem has been apparent with natural Ge for it contains 7.8% of ^{73}Ge (I=9/2). The superhyperfine interaction with ^{73}Ge leads to strong line broadening preventing researchers from obtaining high resolution EPR spectra. However, this can be improved by growing Ge crystals with no ^{73}Ge. In 1964 Wilson demonstrated a significant improvement in EPR signals arising from Ge:As by using an

isotopically enriched ^{74}Ge sample depleted of ^{73}Ge [59]. Fig. 5.3 compares the EPR spectra of arsenic donors in isotopically enriched Ge with spectra of normal Ge [59]. In this case the isotopically enriched ^{74}Ge crystal contained only 0.86% ^{73}Ge. It is clear that the arsenic spectrum obtained with natural Ge is broadened by the presence of ^{73}Ge whereas the spectrum of the ^{74}Ge crystal is very sharp. Therefore, isotopically controlled Ge with low ^{73}Ge content will be extremely useful in the EPR studies of a variety of defects in Ge.

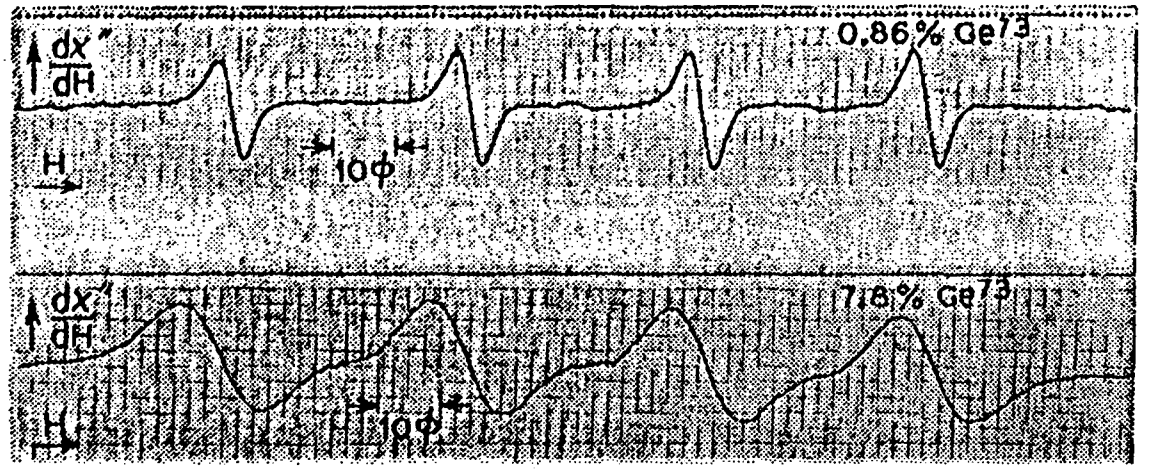

Fig. 5.3 EPR spectrum of Ge:As with different ^{73}Ge composition

5.1.6 Study of the Se double donor in Ge

Selenium (Se) is Group VI element and acts as a double donor in Ge when it substitutes for Ge on a lattice site. However, normal doping methods (melt doping, ion implantation, thermal diffusion, etc.) have met with limited success at introducing Se atoms at the Ge lattice sites. (Instead Se appears to occupy Ge interstitial sites or precipitate.) In order to introduce Se atoms at Ge lattice sites, it may be possible to use isotopically enriched ^{76}Ge crystals and the NTD method. Application of NTD will transmute ^{76}Ge to

^{77}Se. Because thermal neutrons are transmuting ^{76}Ge occupying lattice sites, the products ^{76}Se are likely to reside near the original lattice sites. Unavoidable fast neutrons will damage the crystal and may displace some of the Se atoms. Nevertheless, subsequent annealing will heal the damage and a large fraction of Se atoms may return to Ge lattice sites. A number of semiconductor characterization techniques (DLTS, infrared absorption, EPR, etc. [57]) will be applied to study Se double donors in Ge for the first time.

5.2 Phonon related topics

Because all five stable Ge isotopes have different masses, crystals grown from the various isotope mixtures will exhibit different vibrational properties. In this section the isotope shifts of a few basic properties of Ge due to the change of phonon frequencies will be briefly explained.

5.2.1 Isotope shift of the phonon frequencies - Raman spectroscopy

Among the fundamental vibrational properties of a solid are the frequencies of the characteristic phonons. Two major techniques to measure frequencies of phonons are neutron scattering and Raman spectroscopy [8, 60]. Fig. 5.4 shows phonon dispersion relations of natural Ge (80K, [111] direction) obtained by neutron inelastic scattering by G. Nilsson et al. [8]. The corresponding longitudinal optical (LO) and traverse optical (TO) phonon energies are 31 meV and 37.7 meV, respectively. Using the simple harmonic oscillator approximation, we expect phonon frequencies to be proportional to $M^{-1/2}$ (M: mass of the atom). Shown in Fig. 5.5 are the first order Raman spectra of ~96% ^{70}Ge and of natural Ge crystals grown in for this thesis [21]. The well known TO phonon peak of natural Ge (37.7meV) appears at the wave number ~304.5 cm^{-1}. The average atomic mass of natural Ge is 72.7. The simplest method to estimate the TO phonon peak of ^{70}Ge in wavenumber k_{70} is to employ the relation $k \propto M^{-1/2}$. Thus,

$$\sqrt{\frac{72.7}{70}} = \frac{k_{70}}{304.5} \Rightarrow k_{70} \approx 310 \text{ cm}^{-1} \tag{5.8}$$

The actual peak position of ^{70}Ge in Fig. 5.5 appears at 309.3 cm^{-1} which is very close to the estimate from Eq. 5.8. The small difference between the estimated and measured value is an error due to the mono-atomic approximation in the case of natural Ge. For the rigorous calculation, isotopic disorder must be taken into account. The detailed description of the isotopic disorder effect, peak width calculations, and second order Raman spectra is given in the original paper [21].

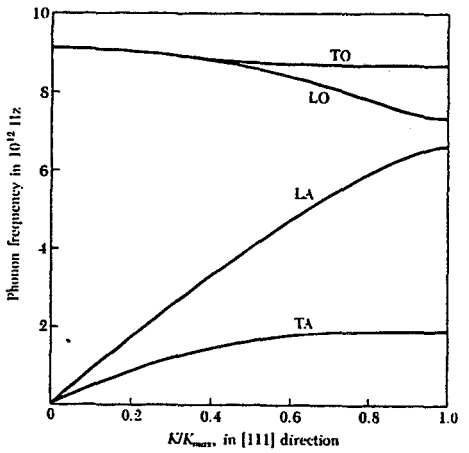

Fig. 5.4 Phonon dispersion relations in [111] direction in Ge

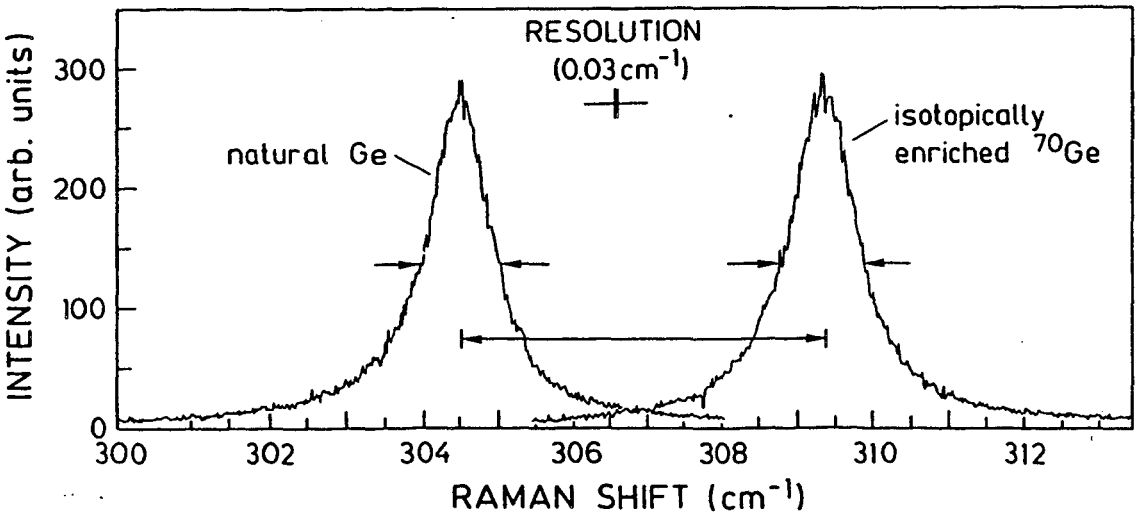

Fig. 5.5 First order Raman spectra of ~96% ^{70}Ge and of natural Ge crystals

5.2.2 Isotope shift of the band gap

The temperature dependence of the energy gap E(T) of semiconductors is generally given by [3,4],

$$E(T) = E' + \int d\omega\, f(\omega)\, \{n(\omega,T) + \frac{1}{2}\} - s\,(c_{11} + 2\,c_{12})\,\Delta V(T)\,/\,3V \qquad (5.9)$$

where n(w, T) is the Bose-Einstein occupation number, $f(\omega)d\omega$ the difference in the electron-phonon coupling for the conduction band minima and the valence band maximum for the modes in the frequency range between ω and $\omega+d\omega$, s the change in the energy per unit compressional hydrostatic stress, c_{11} and c_{12} the elastic constants, and $\Delta V(T)/V$ the fractional volume expansion. At 0K, the energy gap is

$$E\,(T=0) = E' + \frac{1}{2}\int d\omega\, f(\omega) \qquad (5.10)$$

In Eq. 5.9, the second term is a contribution from the electron-phonon interaction whereas the third is a contribution from the lattice constant. Since both quantities are dependent on the isotope mass, the energy gap of the semiconductor itself exhibits an isotope shift. Collins et al. have measured the isotope shift of the indirect energy gap between ^{12}C and ^{13}C diamonds with a photoluminescence technique.*3 This technique involves the detection of an optical transition (luminescence) from an excited electronic state to a lower electronic state. The excitation to the higher state is done by external photon sources (usually a laser). Collins et al. measured the energy shift of boron bound exciton peaks between ^{12}C and ^{13}C which is due to the shift of the band gap. As a result of the isotope substitution, the energy gap of ^{13}C increased by ~13.6 meV over that of natural diamond (98.9%^{12}C) [3, 4]. (The energy gap of the natural diamond at room temperature is

*3 A review of this technique is given in Ref. 53

~5.47eV.) This isotope shift of the gap was determined by a comparison of the boron impurity bound exciton lines in ^{12}C and ^{13}C.

The same method can be applied to determine the isotope shift of band gap in Ge. The difficulty of the accurate band gap shift measurement in the case Ge is due to the extremely small shift value (~1meV predicted between ^{70}Ge and ^{74}Ge [61]), which is a order of magnitude smaller than the case of ^{12}C and ^{13}C. One reason for this is the band gap of natural Ge (~0.65eV) being one order of magnitude smaller than that of diamond (~5.47eV). Also the shift of band gap due to the isotope shift of the lattice constant is small compare to the case of diamonds. For example, the fractional isotope shift of the lattice constant ($\Delta a/a$, a: lattice constant) between ^{74}Ge and natural Ge is on the order of 10^{-5}~10^{-6} [7] which is 1~2 order of magnitude smaller than that of diamond (between ^{12}C and ^{13}C) [6].

Nevertheless, shown in Fig.5.6 are the first results of free exciton spectra recorded with the isotopically enriched ^{70}Ge#4 and ^{74}Ge#2 samples. These spectra were taken by

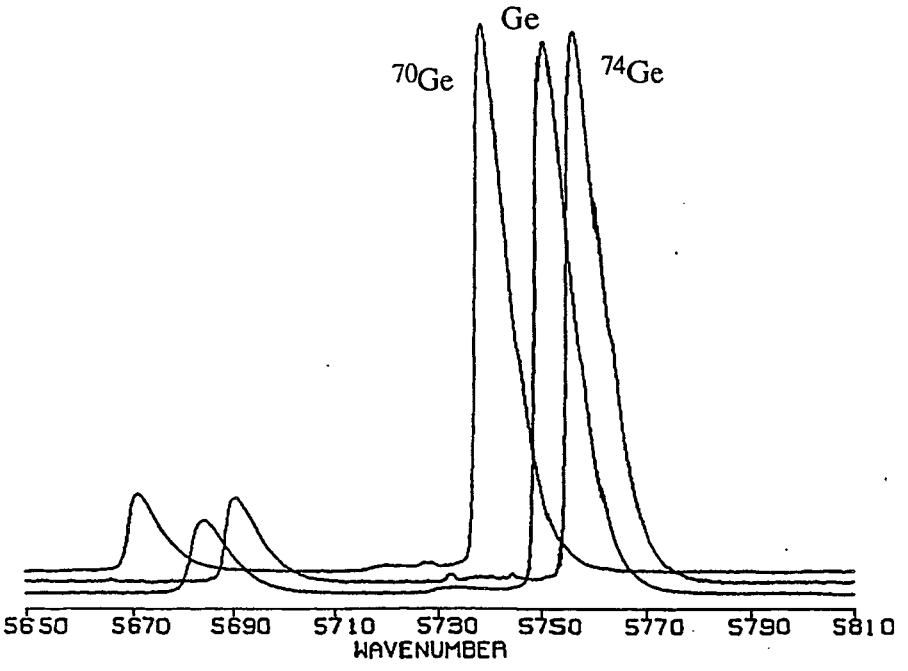

Fig. 5.6 Free exciton photoluminescence spectrum of ^{70}Ge, ^{74}Ge and natural Ge

our collaborators G. Davies et al. who earlier measured the energy gap shift of the diamond mentioned above. In Fig. 5.6, the free exciton peaks of ^{70}Ge and ^{74}Ge appear at approximately 5738 and 5757 cm^{-3} wavenumber, respectively. Because $E=khc/2\pi$ we can replace E with a wavenumber k in Eq. H.1 in Appendix H. Then we obtain the following expression for the photoluminescence free exciton peak shift Δk between ^{70}Ge and ^{74}Ge in wavenumber.

$$\Delta k = k(^{74}Ge) - k(^{70}Ge) = k_g(^{74}Ge) - k_g(^{70}Ge) - k_{\hbar\omega}(^{74}Ge) + k_{\hbar\omega}(^{70}Ge) \quad (5.11)$$

Thus the isotope shift of the energy gap Δk_g between ^{70}Ge and ^{74}Ge in terms of wavenumber becomes,

$$\Delta k_g = k_g(^{74}Ge) - k_g(^{70}Ge) = k(^{74}Ge) - k(^{70}Ge) + k_{\hbar\omega}(^{74}Ge) - k_{\hbar\omega}(^{70}Ge) \quad (5.12)$$

Now substitution of $k_{\hbar\omega}(^{70}Ge) \sim 309.3\ cm^{-1}$ (measured with Raman spectroscopy) and $k_{\hbar\omega}(^{74}Ge) \sim 300.8\ cm^{-1}$ (estimated with Eq. 5.8) yields,

$$\begin{aligned} \Delta k_g &= k_g(^{74}Ge) - k_g(^{70}Ge) \\ &= 5757 - 5738 + 300.8 - 309.3\ (cm^{-1}) \\ &= 10.5\ cm^{-1} \end{aligned} \quad (5.13)$$

Then the isotope shift of the energy gap between ^{70}Ge and ^{74}Ge can be expressed in energy ΔE_g by conversion $\Delta E_g = \Delta k_g hc/2\pi$, i.e.,

$$\Delta E_g = E_g(^{74}Ge) - E_g(^{70}Ge) \sim 1.3\ meV. \quad (5.14)$$

The result obtain in Eq. 5.14 is a rough estimate from the primary result, nevertheless, it is in very good agreement with the calculated value of this isotope shift by Zollner et al. [61]. In order to improve the resolution, the impurity bound exciton photoluminescence will be made with G. Davies et al. in the future.

5.2.3 Isotope shift of the heat capacity

Heat capacity at constant volume C_V is generally given by the Debye formula [9],

$$C_v = \frac{3\,k_D^3}{2\,\pi^2} \int_0^{\Theta_D/T} \frac{x^4\, e^x\, dx}{(e^x - 1)^2} \quad \text{where } x = \frac{\hbar\, c\, k}{k_B\, T} \tag{5.15}$$

where k_D is the radius of sphere in the reciprocal space which contains precisely N allowed vectors (N: number of Bravais lattice sites in the crystal), Θ_D the Debye temperature, and c the velocity of phonon, k the wave vector. Θ_D is defined as,

$$\hbar\, c\, k_D = \hbar\, \omega_D = k_B\, \Theta_D \tag{5.16}$$

where ω_D is the Debye frequency. In the low temperature region ($T<0.2\ \Theta_D$), Eq. 5.15 becomes,

$$C_v = \frac{234\, k_D^3}{6\,\pi^2} \left(\frac{T}{\Theta_D}\right)^3 k_B \tag{5.17}$$

Because the Debye temperature of Ge is ~370 K, Eq. 5.17 is valid below ~77 K. The isotope shift of heat capacity between ^{70}Ge and ^{74}Ge can be estimated by the shift of the Debye frequency, ω_D. Since $\omega_D \propto M^{-1/2}$ and $\Theta_D \propto M^{-1/2}$, one finds $Cv \propto M^{3/2}$ from Eq. 5.17. Therefore we expect the fractional difference of heat capacity $C_V(^{70}Ge)$ and $C_V(^{74}Ge)$ to be,

$$\frac{C_v(^{74}Ge)}{C_v(^{70}Ge)} - 1 = \left(\frac{74}{70}\right)^{\frac{3}{2}} = 8.7\ \% \tag{5.18}$$

To our knowledge, there has been no data published on the isotope shift of heat capacity in Ge up to date.

5.2.4 Isotope shift of the thermal conductivity

In 1958, Geballe and Hull compared the thermal conductivity between isotopically enriched ^{74}Ge and natural Ge crystals [2]. While they observed heavily diffused thermal

conduction in natural Ge due to the random distribution of five stable isotopes, thermal conduction in ^{74}Ge showed a $K=0.06T^{-3}$ dependence below 5K which is known as the Casimir's limit regime [2]. In this regime, phonons experience no scattering from one end of the sample to the other. Therefore the isotopically enriched samples will be ideal samples to investigate various thermal conduction scattering centers and their cross sections.

5.2.5 Low temperature ballistic phonon transport - Phonon focusing

As explained in the previous section, the mean free path of phonons becomes very large at low temperature and the velocity of phonons become comparable with the speed of sound. These extremely fast phonons are called ballistic phonons and the study of their transport is very important for the development of phonon mediated particle detectors. It is also very important for the basic understanding of crystal lattice properties. The propagation of ballistic phonons strongly reflects the anisotropy of the crystal. (The anisotropic propagation of phonons is known as the "phonon focusing effect" [62-64].) However, for the same reason as in the case of thermal conduction, ballistic phonons experience heavy isotope scattering in natural Ge. Therefore, isotopically enriched Ge crystals will be extremely useful in the study of ballistic phonon transport and phonon focusing.

Appendix A: Effective distribution coefficient

With the aid of the binary phase diagram in Fig. A.1, the equilibrium distribution coefficient is defined as follows. For simplicity, we define the horizontal axis of Fig. A.1 as the solute concentration in germanium. When the system is at temperature T, the solute concentrations in the Ge solid (C_S) and in the Ge liquid (C_L) are given by the intersection of the tie line with the solidus and liquidus lines respectively. Then the equilibrium distribution coefficient k_o is defined as

$$k_o = C_S / C_L. \tag{A.1}$$

The value of k_o can be either greater than equal or less than one depending on the phase diagram of the solute impurity with Ge. For the case of the actual zone refining process, the equilibrium distribution coefficient k_o has to be replaced by the effective distribution coefficient since it is a non-equilibrium process. In 1953 Burton, Prim, and Slichter assumed the solid-solute-liquid reaction to be mainly dependent on a diffusion-governed transport process and derived the effective distribution coefficient k_{eff} [65]. They

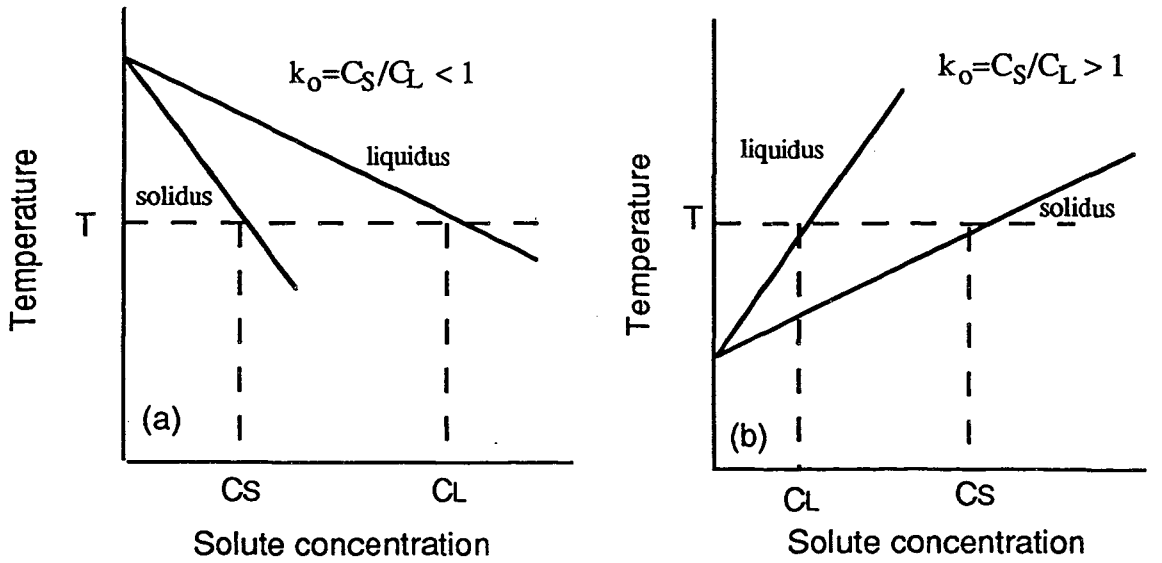

Fig. A.1 Schematic solvent - solute phase diagram
(a) $k_o < 1$ (b) $k_o > 1$

started with the one-dimensional, steady-state diffusion equation of solute atoms across the interface in the liquid moving away from the solidification front in the absence of mixing in the liquid,

$$D \frac{d^2 C}{d x^2} - v_x \frac{d C}{d x} = 0 \tag{A.2}$$

where D is the diffusion coefficient of the solute, C the concentration of the solute, and v_x the velocity of the solidification front in the x direction. The actual solute distribution for $k_o<1$ at the interface is shown in Fig. A.2. The excess "pile up" of the solute concentration on the liquid side is due to the rejection rate of the solute from solidifying Ge being much faster than the rate of the diffusion of the solute in the liquid. The boundary conditions for Eq. A.2 then become

$$C = C_{L(0)} \text{ at } x=0 \quad \text{and} \quad C = C_L \text{ at } x=\delta. \tag{A.3}$$

Then the solution of Eq. A.2 is given by

$$k_{eff} = \frac{k_o}{k_o + (1 - k_o) \exp(-f\,\delta / D)} \tag{A.4}$$

where k_o in this case is given by $C_S/C_L(0)$ and f is the velocity of the solidification.

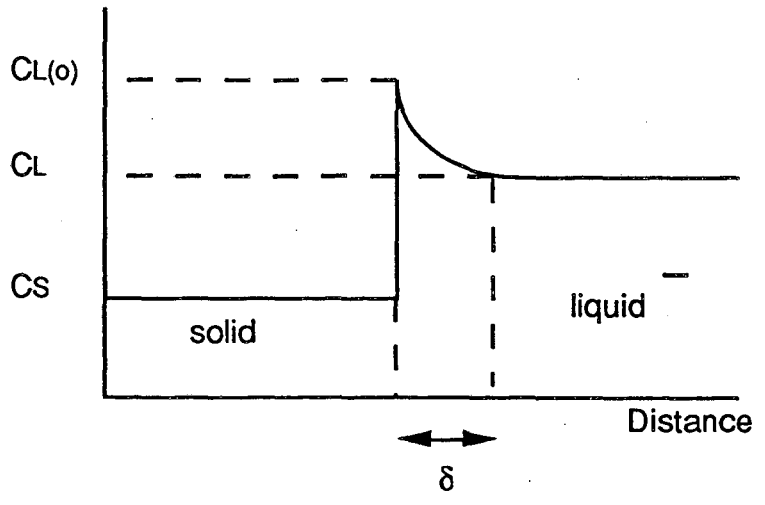

Fig. A.2 Concetration of solute when $k_o < 1$

Appendix B: Secondary Ion Mass Spectroscopy (SIMS)

In our measurement a gallium ion beam was accelerated onto the surface of the sample in order to sputter some of the Ge atoms from the surface. A fraction of the removed Ge atoms was in the form of secondary ions analyzed by a mass spectrometer and separated according to their mass to charge ratio (m/q). The mass spectrometer data was obtained in the form of a number of counts for each value of m/q ratios; consequently, by comparing the count for each Ge isotopes, we determined the isotopic composition of ^{70}Ge#4 and ^{74}Ge#2 crystals. Ref. 57 contain further description of SIMS measurement on semiconductor materials.

Appendix C: Determination of crystal orientation by optical reflection

The system employed in this work is the The tail end of each Ge crystal was lightly abraded with a #240 SiC sand paper to create a small area with a rough surface. The surface was etched with a H_2O:HF:H_2O_2 (4:1:1) solution for 2 minutes. This process preferentially etched the {111} planes of the Ge surface and created a large number of shiny {111} mirrors. A parallel beam of white light was focused on the surface, and the pattern formed by the light reflecting from the sample surface was observed. To find the orientation of the sample, we tilted the crystals and looked for a patterns consisting of specific symmetries, i.e., four-fold and three-fold for <100> and <111> directions, respectively. Finally the direction of crystals was determined by using the standard stereographic projection for the cubic system [66].

Appendix D: Dislocation etching

The experimental steps to obtain dislocation etch pits on {111} planes are the followings;

(1) Cut wafer on exact (111) plane.

(2) Lap with mixture of 9 μm diameter SiC particles and water to produce smooth flat surface.

(3) Etch with HNO_3:HF (4:1) solution to obtain a polished, defect free surface.

(4) Boil in ferricyanide {111} preferential etching solution (6g KOH, 4g $K_3Fe(CN)_6$, and 50 ml H_2O) for ten minutes.

Because dislocations are surrounded by local stress, the step (4) preferentially etches the Ge near dislocations and creates triangular shape etch pits. Therefore the area density of dislocations intersecting with the (111) plane under observation can be found by counting the number of etch pits. Dislocation lines in diamond lattices lie on {111} planes. Since surface of the sample was one of four {111} planes, only the dislocations lying on the rest of three {111} planes could intersect with the (111) plane under investigation. Consequently, dislocation density was calculated by the area density multiplied by 4/3.

Appendix E: Net impurity profile measurement with the resistivity technique

Electrical contacts were formed at intervals of length l=3mm along the growth direction of the ingots by simply rubbing indium-gallium eutectic liquid on the surface. This method is known to produce quite reliable p-type ohmic contacts. A constant current I was sent through the crystals (e.g. 100 μA) and the voltage drop ΔV at each 3 mm interval was measured at 77K in the dark. This temperature was chosen because the generation of electron-hole pairs across the band gap significantly exceeds the extrinsic carrier concentration at the room temperature when Ge crystal has less than $10^{13}cm^{-3}$ electrically

active impurities. With the knowledge of the cross section A of the ingots, the resistivity ρ for the each section of the ingots was determined by the relation $\rho = AR/l = A\Delta V/Il$ where R is the resistance. Then the net-concentration $|N_A - N_D|$ for every 3mm interval can be estimated with the equation $|N_A - N_D| = 1/\rho\mu q$ where μ is the mobility (~40,000 $cm^2/Vsec$ for both electrons and holes at 77K) and q the electron charge ($1.6 \times 10^{-19}C$).

Appendix F: Temperature dependence of the conduction mechanism in doped semiconductors

Fig. F.1 (a) and (b) schematically show an example of the temperature dependence of the carrier concentration and resistivity of a moderately doped and compensated semiconductor. For simplicity we shall discuss a semiconductor which contains a shallow donor impurity concentration N_D with a lower concentration of compensating acceptors N_A. The compensation ratio is defined as N_A/N_D. An analogous explanation applies to p-type semiconductors.

Segment 1 in Fig. F.1: High temperature region ($k_BT>E_g$, E_g: energy gap)

This is the intrinsic region where the temperature is high enough to excite electrons from the valence band to the conduction band to create free electrons and holes in excess of the dopant related electrons. The number of free electrons and holes overwhelm the number of extrinsic carriers, and the slope of ln (n) vs. 1/T in Fig.F.1 (a) is proportional to $E_g/2k_B$.

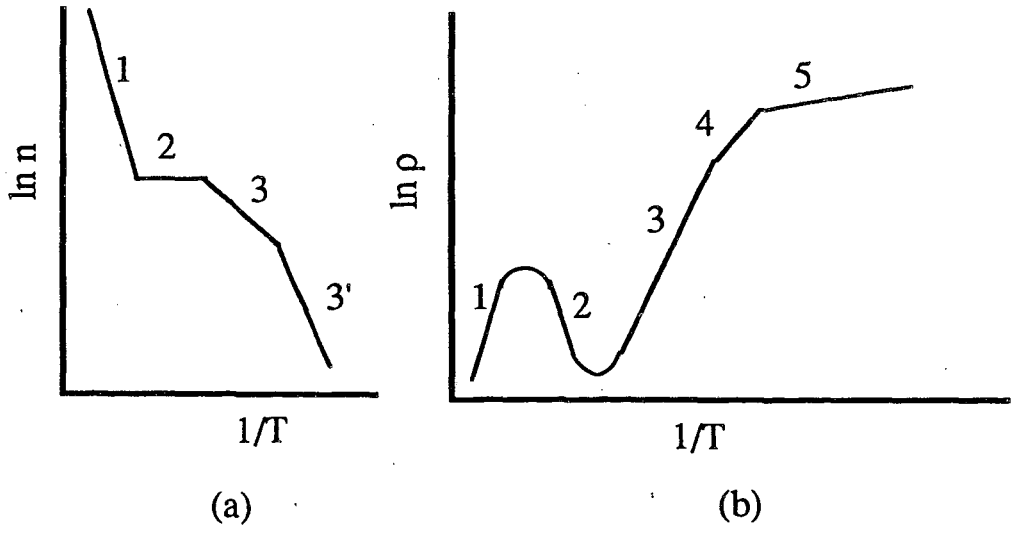

Fig. F.1 Temperature dependence of (a) carrier concentration and (b) resistivity in semiconductors

The resistivity ρ is given by;

$$\rho = (n_e\, q\, \mu_e)^{-1} + (n_h\, q\, \mu_h)^{-1} \qquad \text{(F.1)}$$

where n_e and n_h are the free electron and hole concentrations, q the charge and $\mu_{e,h}$ the mobilities of electrons and holes, respectively. Due to the rapid decrease in the free carrier concentration, the resistivity increases as the temperature decreases.

Segment 2 in Fig. F.1: Extrinsic impurity saturation region ($k_BT>E_D$, E_D: donor ionization energy ~10meV for Ge)

The plateau of segment 2 in ln (n) - 1/T is due to the extrinsic carrier concentration which exceeds the intrinsic free carrier concentration. The temperature is too low to create a large concentration of intrinsic free carriers but sufficient to ionize all n-type shallow impurities. Thus the carrier concentration stays constant at N_D-N_A. The resistivity, on the other hand, decreases as the temperature is lowered because the mobility μ increases when the compensation is relatively low due to a decrease of scattering by lattice vibrations. In Eq. F.1, n and q are constant and μ increases hence, ρ increases as T decreases.

Segment 3 in Fig. F.1: Freeze out region ($k_BT\leq E_D$)

The temperature becomes low so that the thermal energy is not sufficient to maintain the ionization of all donor impurities. Although the temperature dependence of carrier concentration can be rigorously calculated by carrier freeze-out statistics, only the relevant results will be stated here. For detailed description the text by J. Blakemore should be consulted [29]. As the temperature is lowered, the carrier concentration decreases. The behavior of segment 3 in the ln (n) -1/T curve strongly depends on compensation level. If the material is uncompensated, the slope is proportional to $E_D/2k_BT$ throughout segment 3. If the material is compensated ($N_A\neq 0$), the slope is proportional to $E_D/2k_BT$ in the temperature range for which $n>N_A$. For $n<N_A$ the slope is proportional to E_D/k_BT. In Fig. F.1 (a) segment 3 is half slope ($\propto E_D/2k_BT$) and 3' is full slope ($\propto E_D/k_BT$). The kink in slope occurs at the minority impurity concentration level N_A. The resistivity, as seen in Fig. F.1 (b), increases due to the rapid decrease of the carrier concentration.

When the dopant concentration in a semiconductor is relatively low, the thermal excitation of carriers from the donor levels to the conduction band generates the conducting electrons. However, when a semiconductor is moderately to highly doped ($>10^{15}cm^{-3}$ for Ge), completely different conduction mechanisms begin to dominate at very low temperatures.

Segment 4 in Fig. F.1 (b): ε_2 conduction.

When a semiconductor contains a relatively large concentration of impurities ($3X10^{17}>N_D-N_A\geq10^{16}cm^{-3}$ for Ge) with very little compensation, so called "ε_2 conduction" dominates. Electrical conduction in this case is no longer due to free carriers in the conduction band, but is due to electrons excited to the so called "upper Hubbard" band. Because electrons transfering charges in this case are not "free" electrons in conduction band, it is useless to consider Fig. F.1 (a). Gershenzon et al [67] showed that neutral donors in Ge can bind a second electron (the D^- state) with a binding energy of the order of $0.1E_D$. This is analogous to the formation of H^-. Because the binding energy of the state is small, the D^- state has a very large Bohr radius. The overlap of D^- wavefunctions leads to an energy band at the energy between the donor levels and

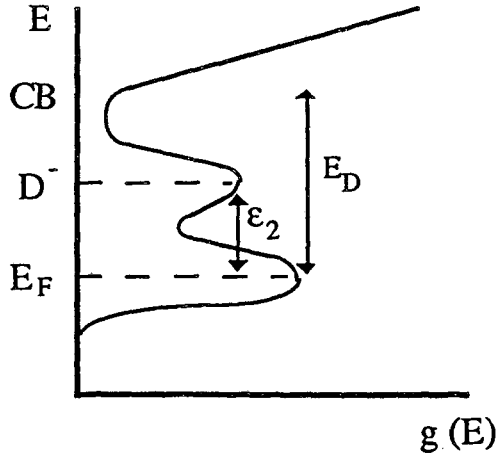

Fig. F.2 Density of states of the D^-band and the activation energy for the ε_2 conduction

conduction band minima (CB) as shown in Fig. F.2. Since $\varepsilon_2 < E_D$, this conduction mechanism dominates at lower temperatures at which normal freeze out would occur otherwise. In order for this ε_2 conduction to occur, the donor concentration must be high enough so that D^- states can overlap. Also a lower compensation ratio is favorable for the ε_2 conduction since compensation reduces the number of electrons in the donor states and decreases the probability for D^- state formation.

Segment 5 in Fig. F.1.(b): Hopping conduction regime.

Further decrease in temperature may lead to the occurrence of hopping conduction. Whether or not it occurs depends on the donor and acceptor impurity concentrations. When these impurity concentrations are sufficiently high ($3X10^{17} > N_D - N_A \geq 10^{15} cm^{-3}$ for Ge), electrical conduction is due to hopping of electrons between donor impurity sites. The resistivity slope changes in segment 5 of Fig. F.1 (b) is due to hopping conduction.

At the high temperature side of the hopping conduction regime, one usually observes "nearest neighbor hopping."

Hopping of electrons occurs between an occupied donor site and an unoccupied donor site. Fig. F.3 shows the example of electrons hopping from occupied sites to the nearest unoccupied sites. In order to create a number of unoccupied donor sites, it is necessary to have compensating acceptors. Electrons prefer the lowest possible energy states hence electrons at donor sites choose to "fall" into all available acceptor sites. This is the essence of "compensation". Once unoccupied states are created, electrons are able to jump into them from the nearest occupied states. This is called nearest-neighbor hopping conduction. Notice that donor states next to each other take slightly different energy levels due to the Pauli exclusion principle and the fluctuation of the potential arising from the compensating centers. The resistivity can be expressed as

$$\rho = \rho_0 \exp\left(\frac{E_A}{k_B T}\right) \tag{F.2}$$

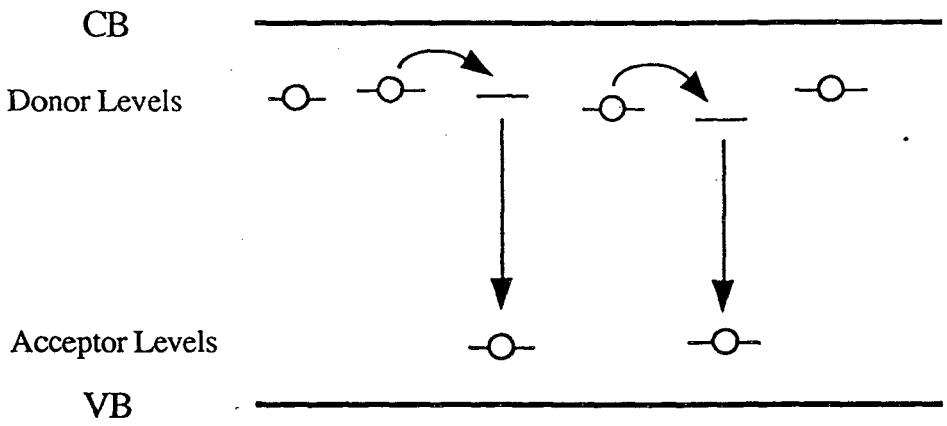

Fig. F.3 Nearest neighbor hopping conduction in n-type semiconductors

where E_A is the activation energy for the hopping, ρ_0 the constant pre-factor.

In the lowest temperature regime, where the available thermal energy is less than the nearest-neighbor hopping activation energy E_A, electrical conduction occurs by electrons jumping to sites which are energetically in reach, though they may be much further away. This is called variable range hopping conduction. The mechanism is shown in Fig. F.4. Each electron sitting on the donor site "looks" for an empty donor site into which the electron can hop with the available thermal energy k_BT. In Fig. 2.6 the electron at site 1 finds the state at site 6 to be within energy k_BT; so it can hop from site 1 to 6, whereas site 5 is out of the available k_BT range even though it is closer than site 6. The theory of variable range hopping conduction predicts the following temperature dependence of resistivity [38,39]

$$\rho = r_0 \exp\left(\frac{T_0}{T}\right)^N \quad \text{where } N = \frac{1}{4} \sim \frac{1}{2} \tag{F.3}$$

In the case of a NTD germanium, N is found to be 1/2.

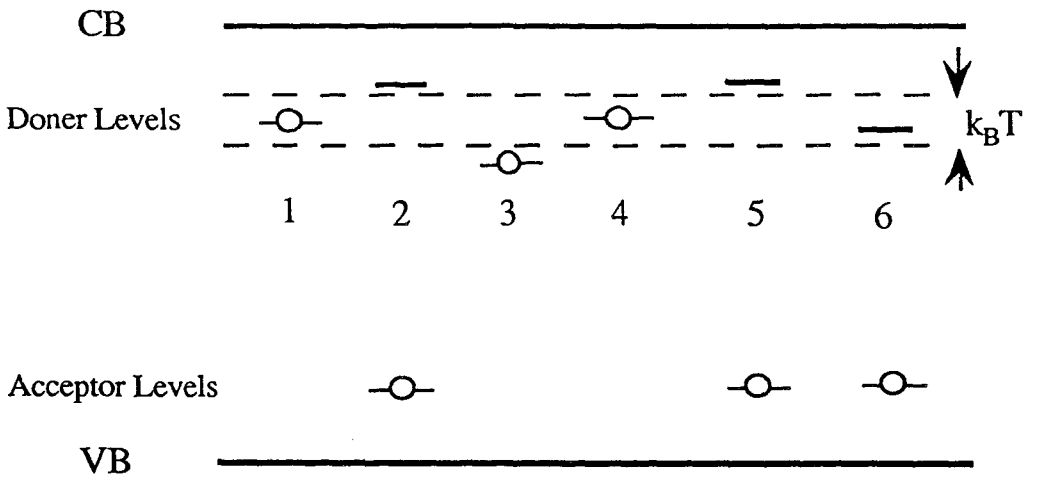

Fig. F.4 Variable range hopping conduction in n-type semiconductors

Appendix G: Photothermal ionization spectroscopy (PTIS)

Photo Ionization Spectroscopy (PTIS) of impurities in a semiconductor involves the ionization of impurities in two steps. This two-step process is schematically shown in Fig.G.1 for the case of a donor. An electron in the ground state of the donor is excited to one of the excited states by the incident photon of energy $\Delta E = h\nu$. Subsequently, the ambient temperature contributes the phonon energy $h\omega$ to excite the electron from the excited state to the conduction band. These free electrons in the conduction band are detected through an increase in the conductivity of the crystal. Two ohmic contacts applied to opposite surfaces of the sample are used to measure the conductivity. Usually a PTI spectrum is taken under an appropriate fixed temperature with the incident nearly monochromatic photon flux (infrared for the case of Ge) produced from the broad band light source by a Michelson interferometer. Because PTIS is base on an electrical measurement, this method has excellent sensitivity in which detection of a shallow impurity concentration as low as $\sim 10^7 cm^{-3}$ may be possible in favorable cases [68].

Identification of shallow impurities with PTIS is quite simple. Since electron (or hole) transitions within each shallow donor (acceptor) occur with characteristic photon energies, the identity of impurities can be determined by observing the peak positions of the PTI signal arising from each of the characteristic transitions.

The theoretical determination of electron (hole) transition energies within shallow impurities in semiconductor relies on the "effective mass theory (EMT)" [69] which describes the energy states of a local charge bound to a particular impurity. Shallow impurities are often called "hydrogenic" because an electron (or hole) is bound to singly-charged donor (or acceptor) core as in the case of a hydrogen atom. Thus the Bohr equation for the hydrogen atom with an appropriate effective mass m^* of a electron (or hole) and dielectric constant ε of a host semiconductor provides a good estimate for the

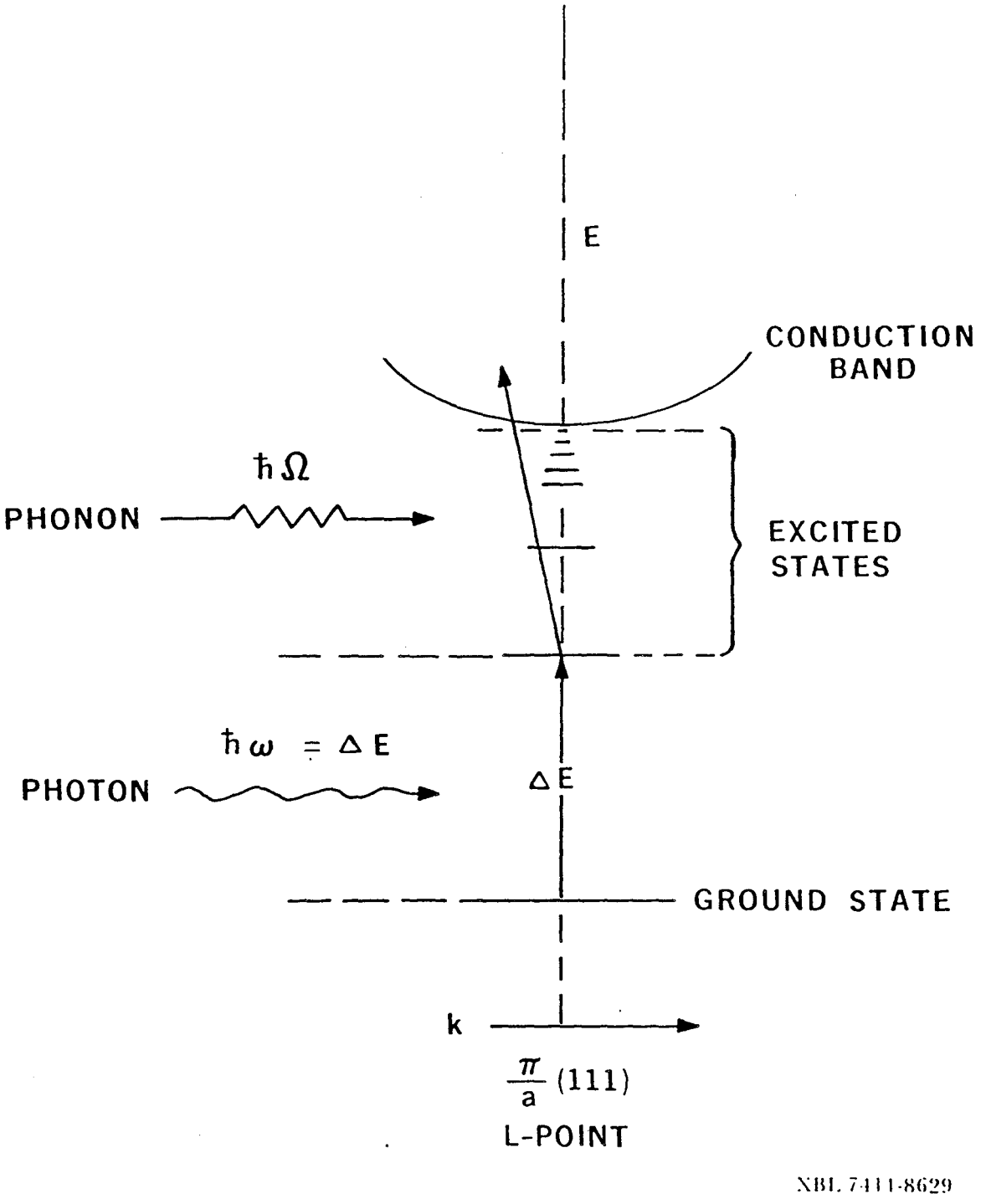

Fig. G. 1 The two-step absorption process which leads to photothermal ionization

ground state energy of bound electron (or hole):

$$E = -\frac{4\pi^2 e^4 m^*}{\varepsilon h^2} \tag{G.1}$$

where e is the charge of the electron (hole) and h is Planck's constant. Following this EMT calculation, the ground state energy of a shallow donor in Ge was found to be ~9.9meV [70]. The Bohr radius r of the ground state (s-like) wave function of a shallow impurity can be also calculated by the following equation based on the Bohr hydrogen model:

$$r = \frac{\varepsilon h^2}{4\pi^2 e^2 m^*} . \tag{G.2}$$

The Bohr radius is ~80Å for Ge which means that the 1s ground state wave function extends over more than 1000 Ge lattice sites in the crystal. Excited states extend over even larger volumes. Fig. G.2 shows the energy levels of a group III acceptor in Ge. The ground state ($^1S_0$ in the spectroscopic term) has the $1\Gamma_8^+$ symmetry of the valence band top and the transitions to the p-like excited states are denoted by the letters G, D, C, etc. In Fig. G.2, the ground state energies differ among various shallow impurities since the s-like wave function with the probability density maximum at the impurity core is strongly affected by the core potential of the specific impurity. On the other hand the p-like wave function has a probability density zero in the impurity core and is only shaped by the Coulomb field of the point core potential. Consequently the p-like wave functions are almost independent of the chemical nature of the impurity core while excited states are virtually identical for all shallow donors and for all shallow acceptors. This can be readily seen in Fig. G.2 as the energy spacings between p-like excited states (spacing between $1\Gamma_8^-$, $2\Gamma_8^-$, $1\Gamma_7^-\otimes 3\Gamma_8^-$, etc. and even up to the valence band) are identical for different shallow acceptors.

Following the EMT, the energy (i.e., wave number) spacings between excited state energy peaks (G, D, C, etc.) are equal for all shallow acceptors but the energy position of a particular peak (say C transition peak) for different acceptor relative to the valence band

edge is different due to the shift in the ground state energies. This leads the transitions within each impurity to occur precisely at their characteristic photon energies, i.e., PTIS is a very powerful technique for the identification of impurities in semiconductor.

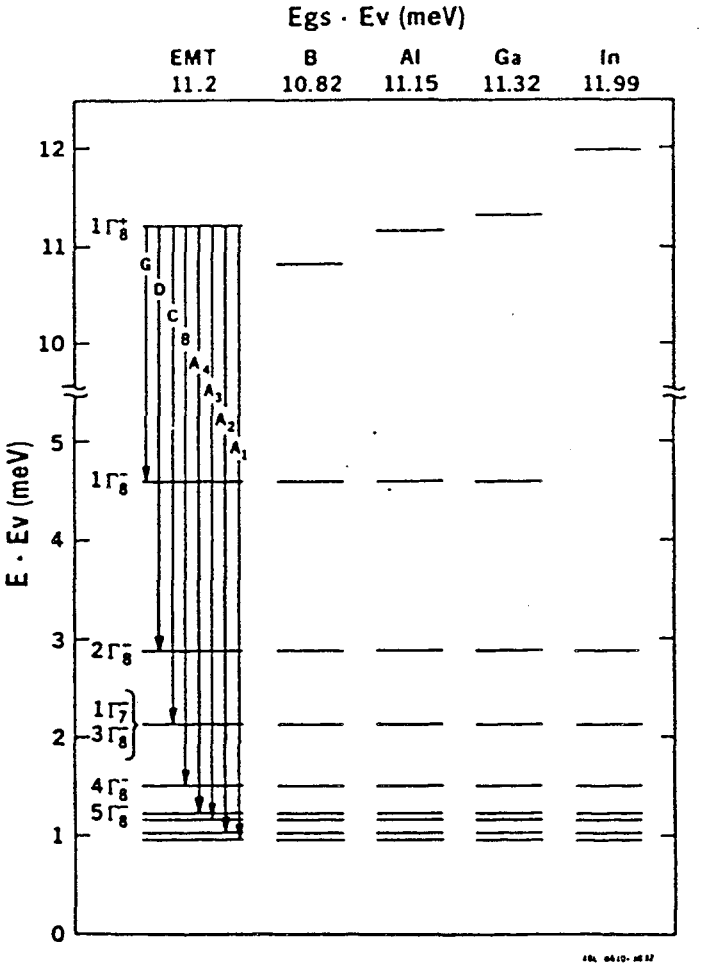

Fig. F.G.2 The energy levels for the ground state and lowest-lying odd-prity excited states of Group III acceptors in Ge

Appendix H: EPR measurement

An application of an external magnetic field, H, induces alignment of magnetic dipoles to spin parallel and anti-parallel. This is the well known Zeeman splitting of a paramagnetic state by an external field (see Fig. H.1.a). The splitting of two Zeeman levels in the case of a defect with isotropic single unpaired spin is given by,

$$\Delta E = g\,\mu_B\,H \tag{H.1}$$

where ΔE is the energy difference between two levels, g the g-tensor which reflects the symmetry of the defect, μ_B the Bohr magnetron, and H the applied external field. When the crystal is subjected to incident microwave radiation of a fixed frequency ν, the radiation

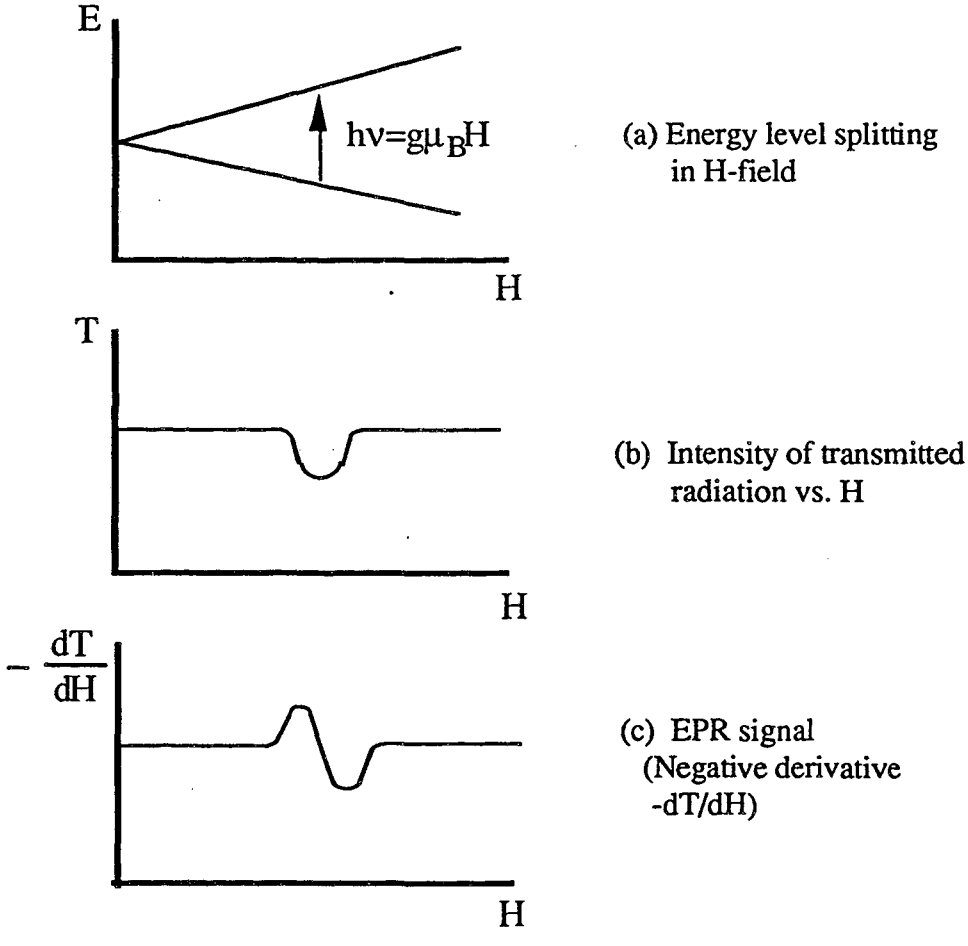

(a) Energy level splitting in H-field

(b) Intensity of transmitted radiation vs. H

(c) EPR signal (Negative derivative -dT/dH)

Fig. G.1 EPR spectroscopy

is absorbed when the following condition is satisfied for a particular H;

$$\Delta E = h \nu \tag{H.2}$$

Fig. H.1.b shows the intensity of transmitted radiation. Notice the dip at the field which satisfies Eq. H.2. The EPR spectrum is obtained by taking the negative derivative of the transmission signal -dT/dH (Fig. H.1.c.). Generally, EPR signals are further complicated by the following effects. When defects are anisotropic, direction dependence of the EPR spectrum appears and evaluation of the g-tensor in Eq. H.1 is necessary. The hyperfine interactions between the nuclear magnetic moment of the defect and the paramagnetic electron will give rise to dipolar field H_{Int}. Due to these internal fields, the EPR lines are displaced along the H direction or replica of the original spectrum are created along the H direction. The superhyperfine interaction is the hyperfine interaction between nuclear spins of the neighboring host lattice atoms and the paramagnetic electron of the defect. The complication due to the superhyperfine interaction can be very serious especially when the host atoms of high value nuclear spin are randomly distributed in the crystal. Thus the nuclear spins of host lattice atoms play a very important role in the EPR study of impurities and defects. Natural Si contains 4.7% of ^{29}Si with nuclear spin I=1/2. The low spin of ^{29}Si and the small concentration of ^{29}Si make Si as a better material to investigate with the EPR. However, each resonance line of the Si EPR spectrum is normally accompanied by weak satellites due to the unpaired electrons which have one ^{29}Si neighbor, and the resonance lines are broaden as well in Si due to presence of ^{29}Si. Germanium is even worse for EPR studies since it contains 7.8 % ^{73}Ge which has nuclear spin of 9/2. Therefore previous attempts to study defects using EPR in natural Ge have suffered from poor resolution due to the superhyperfine interactions with ^{73}Ge.

Appendix I: Determination of the isotope shift of the energy gap with the exciton photoluminescence in indirect semiconductors.

When an electron and a hole are bound to each other they form a pair called exciton. When this pair is free to move around within a crystal, it is called free exciton. The binding energy of free excitons in Si is 14.7 meV and in Ge 4.15 meV. The threshold energy E_{th} for the free exciton photoluminescence for the case of an indirect semiconductor is given by,

$$E_{th} = E_g - E_x - \hbar\omega \qquad (I.1)$$

where Eg is the indirect energy gap, E_x the exciton binding energy, $h\omega$ the energy of the momentum conserving phonon necessary in the case of indirect semiconductors.

When excitons are bound to impurities in semiconductors, they form energy levels associated with the impurities. These are called bound excitons. The threshold energy E_{th}' for bound exciton luminescence is given by,

$$E_{th}' = E_g - E_x - E_B \qquad (I.2)$$

where E_B is the binding energy of the exciton to the neutral shallow center (~1/10 of ionization energy of shallow impurity). Among these parameters, E_x and E_B are considered to exhibit no isotope shift. Therefore, one can immediately determine the isotope shift of the gap in comparing bound exciton threshold energy for the crystals of different isotopes. That is $\Delta E_{th}' = \Delta E_g$ since E_x and E_B are constant in Eq. I.2.

References

[1] I. S. Shlimak, L. I. Zarubin, A. N. Ionov, F. M. Vorobkalo, A. G. Zabrodskii, and I. Y. Nemish, Sov. Tech. Phys. Lett. **9**, 377 (1983)

[2] T. H. Geballe and G. Hull, Phys Rev. **110**, 773 (1958)

[3] T. R. Anthony, W. F. Banholzer, J. F. Fleischer, L. Wei, P. K. Kuo, R. L. Thomas and R. W. Pryor, Phys. Rev. B **42**, 1104 (1990)

[4] A. T. Collins, S. C. Lawson, G. Davies, and H. Kanda, Phys. Rev. Lett. **65**, 891 (1990)

[5] A. T. Collins, S. C. Lawson, G. Davies, and H. Kanda, Mod. Phys. Lett. B **5**, 407 (1991)

[6] H. Holloway, K. C. Hass, M. A. Tamor, T. R. Anthony, and W. F. Banholzer, Phys. Rev. B **44**, 7123 (1991)

[7] R. C. Buschert, A. E. Merlini, S. Pace, S. Rodriguez, and M. H. Grimsditch, Phys. Rev. B **38**, 5219 (1988)

[8] C. Kittel, in "Introduction to Solid State Physics", Six Edition, (John Wiley & Sons, New York, 1986)

[9] N. W. Ashcroft and N. D. Mermin, in "Solid State Physics", International Edition, (Sunders College, Philadelphia, 1976)

[10] D. R. Olander, Sci. Am. **239**, 37 (1978)

[11] E. E. Haller and F. S. Goulding, in "Handbook of Semiconductors", Volume 4, edited by C. Hilsum (North-Holland, 1980),

[12] N. Wang, B. Sadoulet, T. Shutt, J. Beeman, E. E. Haller, A. Lange, I. Park, R. Ross, C. Stanton, and H. Steiner, IEEE Trans. Nucl. Sci. **NS-35**, 55 (1988)

[13] B. Sadoulet, T. Shutt, N. Wang, A. Commings, P. Barnes, J. Beeman, J. Emes, Y. Giraud-Heraud, E. E. Haller, A. Lange, J. Rich, and R. Ross, in "Low Temperature Detectors for Neutrinos and Dark Matter III", edited by L. Brogiato, D. V. Camin and E. Fiorini (Editions Frontiers, Gif sur Yvette, 1990)

[14] A. E. Lange, E. Kreysa, S. E. McBride, P. L. Richards, and E. E. Haller, Int. J. IR MM Waves **4**, 689 (1983)

[15] N. M. Haegel, in "Transient and temperature-dependent phenomena in Ge:Be and Ge:Zn far infrared photoconductors", Ph.D Thesis, (University of California, Berkeley, 1985); LBL-20627

[16] N. M. Haegel, M. R. Hueschen and E. E. Haller, Infrared Physics **25**, 273 (1985)

[17] N. M. Haegel, E. E. Haller and P. N. Luke, Int. J. IR MM Waves **4**, 945 (1983)

[18] "Table of Isotopes", Seventh Edition, edited by C. M. Lederer and V. S. Shirley (John Wiley & Sons, New York, 1978)

[19] "Neutron Ttansmutation Doping of Semiconducto Materials", edited by R. D. Larrabee (Plenum, New York, 1984)

[20] R. F. Milligan and G. A. Thomas, Annu. Rev. Chem. **36**, 139 (1985)

[21] H. D. Fuchs, C. H. Grein, C. Thomsen, M. Cardona, W. L. Hansen, E. E. Haller, and K. Itoh, Phys. Rev. B **43**, 4835 (1991)

[22] W. G. Pfann, in "Zone Melting", Second Edition (John Wiley & Sons, New York, 1966)

[23] W. G. Pfann and K. M. Olsen, Phys. Rev. **89**, 322 (1953)

[24] F. A. Trumbore, Bell Syst. Tech. J. **39**, 205 (1960)

[25] G. S. Hubbard, E. E. Haller, and W. L. Hansen, IEEE Trans. Nucl. Sci. **NS-25**, No.1, 362 (1978)

[26] The crucible was made and cleaned by Carbon USA, Ultra Carbon Division, USA.

[27] E. E. Haller, W. L. Hansen, P. N. Luke, R. McMurray and B. Jarrett, IEEE. Trans. Nucl. Sci. **NS-29**, No. 1, 745 (1982)

[28] D. Hull and D. J. Bacon, in "Introduction to Dislocations", Third Edition (Pergamon Press, Oxford, 1984)

[29] J. Blakemore, in "Semiconductor Statistics", Second Edition, (Dover, New York, 1985)

[30] "Growth and Characterisation of Semiconductors", edited by R. A. Stradling and P. C. Klipstein (Adam Hilger, Bristol and New York, 1990)

[31] T. M. Lifshits and F. Ya. Nad, Dokl. Akad. Nauk SSSR **162**, 801 (1965); Soviet. Phys. - Doklady **10**, 532 (1965)

[32] E. E. Haller, W. L. Hansen, and F. S. Goulding, Adv. Phys. **30**, 93 (1981)

[33] Sh. M. Kogan and T. M. Lifshits, Phys. Stat. Sol. A, **39**, 11 (1977)

[34] K. Kuriyama, M. Yanagi, K. Iwamura, Y. Kim, and C. Kim, J. Appl. Phys. **54**, 673 (1983)

[35] N. P. Palaio, S. J. Pearton, and E. E. Haller, J. Appl. Phys. **55**, 1437 (1984)

[36] I. S. Park and E. E. Haller, J. Appl. Phys. **64**, 6775 (1988)

[37] Data compiled by J. Beeman. All NTD Ge samples were fabricated at the Lawrence Berkeley Laboratory, Berkeley, USA.

[38] N. F. Mott, in "Metal-Insulator Transition", Second Edition, (Taylor & Francis, London, 1990)

[39] B. I. Shklovskii and A. L. Efros, in "Electronic Properties of Doped Semiconductors", Solid State Series Vol. 45 (Springer-Verlag, Berlin Heidelberg, 1984)

[40] H. Fritzsche and M. Cuevas, Phys. Rev. **119**, 1238 (1960)

[41] N. F. Mott and W. D. Twose, Adv. Phys. **10**, 707 (1961)

[42] V. P. Dobrego and O. P. Ermolayev, Sov. Phys. Semicond. **9**, 606 (1975)

[43] E. A. Davis and W. D. Compton, Phys. Rev. **A140**, 2183 (1965)

[44] N. F. Mott, Proc. Phys. Soc. **A62**, 416 (1949)

[45] P. P. Edward and M. J. Sienko, Phys. Rev. B **17**, 2575 (1978)

[46] P. W. Anderson Phys. Rev. **109**, 1492 (1958)

[47] E. Abrahams, P. W. Anderson, D. C. Licciardello, and T. W. Ramakrishnan, Phys. Rev. Lett. **42**,695 (1979)

[48] G. A. Thomas, Y. Ootsuka, S. Katsumoto, S. Kobayashi, and W. Sasaki, Phys. Rev. B **25**, 4288 (1982)

[49] M. J. Jirsch, U. Thomanschefsky, and D. F. Holcomb, Phys. Rev. B **37**. 8257 (1988)

[50] T. F. Rosenbaum, R. F. Milligan, M. A. Paalanen, G. A. Thomas, R. N. Bhatt, and W. Lin, phys. Rev. B **27**,7509 (1983)

[51] P. F. Newman and D. F. Holcomb, Phys. Rev. B **28**, 638 (1983)

[52] D. W. Koon and T. G. Castner, Phys. Rev. B **40**, 1216 (1989)

[53] P. F. Newman and D. F. Holcomb, Phys. Rev. Lett. **51**, 2144 (1983)

[54] P. Dai, Y. Zhang, and M. P. Sarachik, Phys. Rev. Lett. **66**, 1914 (1991)

[55] P. Dai, Y. Zhang, and M. P. Sarachik, Phys. Rev. Lett. **67**, 136 (1991)

[56] R. N. Bhatt and T. M. Rice, Phil Mag B **42**, 859 (1980)

[57] "Growth and Characterisation of Semiconductors", edited by R. A. Stradling and P. C. Klipstein (Adam Hilger, Bristol and New York, 1990)

[58] E. R. Weber, "Proceeding of SPIE", edited by F. H. Pollak (Bellingham, 1985), p. 160

[59] D. K. Wilson, Phys. Rev. **134**, A265 (1964)

[60] M. Cardona, in "Modulation Spectroscopy", (Academic Press, New York, 1969)

[61] S. Zollner, M. Cardona and S. Gopalan, Phys. Rev. B **45**, 3376 (1991)

[62] G. A. Northrop and J. P. Wolfe, in "Non-equilibrium Phonon Dynamics", edited by W. E. Bron (Plenum, New York, 1985), p. 165

[63] B. A. Young, B. Cabrera, and A. T. Lee, Phys. Rev. Lett. **64**, 2795 (1990)

[64] S. Tamura, J. A. Shields, and J. P. Wolfe, Phys. Rev. B **44**, 3001 (1991)

[65] J. A. Burton, R. C. Prim, and W. P. Slichter, J. Chem. Phys. **21**, 1987 (1953)

[66] O. Johari and G. Thomas, in "The Stereographic Projection and Its Applications", (John Wiley & Sons, New York, 1969)

[67] E. I. Gershenzon, G. N. Gol'tsman, and A. P. Mel'nikov, JETP Lett. **14**, 185 (1971)

[68] Sh. M. Kogan, Fiz. Tekh. Poluprov. **7**, 1231 (1973), Sov. Phys. Semicond. I, 828 (1973)

[69] C. Kittel and A. H. Mitchell, Phys. Rev. **96**, 1488 (1954)

[70] R. A. Faulkner, Phys. Rev. **184**, 713 (1969)

LAWRENCE BERKELEY LABORATORY
UNIVERSITY OF CALIFORNIA
TECHNICAL INFORMATION DEPARTMENT
BERKELEY, CALIFORNIA 94720